International Journal of
Molecular Sciences

MDPI

Article

RegenaCare: The Smart Bandage from Lab to Skin and Its Applications

Jia Huey Tham [1], Jade Au [2], Pui Ting Wong [1], Muhammad Umer Qureshi [2], Mohammad Mahmoud [1] and Sachin Sharma Ashok Kumar [3,4,*]

[1] Department of Chemical Engineering, School of Engineering, Taylor's University, Subang Jaya 47500, Selangor, Malaysia
[2] Department of Mechanical Engineering, School of Engineering, Taylor's University, Subang Jaya 47500, Selangor, Malaysia
[3] School of Engineering, Taylor's University, Subang Jaya 47500, Selangor, Malaysia
[4] Clean Technology Impact Lab, Taylor's University, Subang Jaya 47500, Selangor, Malaysia
* Correspondence: sachin.sharma@taylors.edu.my

Abstract

Chronic wounds, including diabetic foot ulcers and trauma injuries, require frequent monitoring to detect early infection, but conventional dressings provide only passive protection. The purpose of this paper is to propose a solution for these patients by presenting RegenaCare, a low-cost, proof-of-concept NFC-powered smart bandage with a web-hosted interface displaying preliminary colourimetric and physiological-sensing data. The hydrogel is a polyvinyl alcohol (PVA)-gelatin membrane incorporating aloe vera and roselle (*Hibiscus sabdariffa*) extract to explore roselle's potential for pH-responsive colour change in infection monitoring, with an electronic subsystem comprising an STM32F103C8T6 microcontroller, MAX30100 heart-rate sensor, and ST25DV16K NFC module. Membranes were freeze- or oven-dried and evaluated through swelling, tensile and Fourier-transform infrared (FTIR) spectroscopy tests. Freeze-dried samples had higher swelling ratios. Oven-dried aloe vera-gelatin membranes achieved the highest tensile strength (6.34 MPa), exceeding the 0.5–1.5 MPa target, and FTIR confirmed gelatin-associated amide bands with differences between roselle-containing and control formulations. UV-Vis absorbance likely exceeded the spectrophotometer's upper limit, and the pH colourimetric response was non-monotonic. These results suggest the feasibility of a low-cost (approximately RM51.50 per unit), NFC-enabled smart bandage for exploratory wound monitoring, although its limitations, alongside power delivery and communication performance, require further development before real-world deployment.

Keywords: smart bandage; hydrogel; near-field communication; infection detection; roselle hibiscus extract

Check for updates

Academic Editor: Celia García-Hernandez

Received: 28 September 2026
Revised: 10 November 2026
Accepted: 11 November 2026
Published: 17 November 2026

Copyright: © 2026 by the authors. Licensee MDPI, Basel, Switzerland. This article is an open access article distributed under the terms and conditions of the Creative Commons Attribution (CC BY) license.

1. Introduction

Chronic wounds, including diabetic foot ulcers, pressure ulcers, and venous leg ulcers, affect an estimated 6.3% of the population worldwide, with up to 25% of diabetic patients expected to develop a chronic wound during their lifetime [1]. In Malaysia, the growing prevalence of diabetes has led to a significant burden of diabetic foot ulcer-related hospitalisations and amputations [2]. Trauma and post-operative wounds present a similar challenge, requiring continuous monitoring to prevent infection and delayed healing.

Conventional wound care relies on passive dressings such as gauze, foam, and hydrocolloids that keep a wound protected and moist but provide no diagnostic capability; the

condition of the wound can only be assessed through manual inspection, which delays the detection of infection [1]. A growing body of research has explored smart wound dressings that incorporate biosensors capable of continuously tracking parameters such as pH, temperature, and oxygen levels [3], yet most existing commercial smart bandages remain bulky, battery-dependent, and expensive, limiting patient compliance in everyday use.

Wound pH is a particularly useful diagnostic parameter, since chronic and infected wounds tend to be alkaline (pH 7–9) while healing wounds are mildly acidic [4]. Colourimetric pH indicators, including anthocyanin-based biosensors, have been widely investigated for wound monitoring due to their biocompatibility and visible colour response to pH change [5]. Roselle extract was included because published work has described its bioactive and pH-dependent anthocyanin properties; its antimicrobial activity and wound-contact safety were not evaluated in this study. In parallel, near-field communication (NFC) has emerged as a leading approach for wireless, battery-free data transmission from wearable healthcare devices, enabling monitoring through a mobile application without an onboard power source [6]. Advances in smartphone-based image diagnostics further enable colourimetric analysis of biomarkers directly from a phone camera [7].

Table 1 shows a comparison between RegenaCare and other existing technologies. Temperature and pH are physiological parameters that are often monitored as wound infections often affect them. This is because when wounds are infected, there is an increase in inflammatory factors and a dilation of capillaries. On the other hand, pH also increases due to bacterial infections, causing physiological changes. The worse the infection, the more the pH increases [8]. While there are smart bandages that use colourimetric pH sensing, most works demonstrate pH sensing through electrodes. An addition that is not as common is blood-flow rate and blood type. The MAX30100 sensor was included to monitor blood flow at the dressing site. Beats per minute (BPM), perfusion index (PI) and accelerated photoplethysmography (APPG) give an indication of circulatory status and tissue perfusion, which are relevant because adequate blood flow and oxygen delivery are required for wound healing. Adequate oxygenation of the wound can determine the healing process. Knowing the data may allow doctors to optimize wound perfusion, which can reduce the risk of postoperative infections [9]. In trauma patients, changes in these readings could also help flag poor circulation or excessive blood loss. These readings are indirect, and they do not indicate local wound infection. Blood typing is a separate feature of the smart bandage for general-trauma wounds like car accidents, where severe blood loss is the leading cause of preventable death and many deaths occur before arrival at hospital [10]. While versions for post-surgery wounds may exclude this feature, the goal of blood typing is to help the medical team and ambulance crew. When a patient's blood group is unknown, a rapid ABO/Rh readout from the bandage could help medical teams and ambulance crews arrange a type-specific transfusion sooner. While the common clinical practice is to use Group O RhD negative blood for all emergency transfusions, it offers no extra safety benefits. This becomes a problem when the population with Group O RhD negative blood types only make up a small percentage and clinics have limited resources, as in places like Australia, there are only 6.5% of the population with this blood type and clinics can have up to 17% red blood cells (RBC) of the blood type. Emergency uncrossmatched group O RBC are to be used only in an emergency to save a patient's life and when there is no current valid pretransfusion specimen, not to just save time. The National Blood Authority in Australia recommends minimizing the need for uncrossmatched group O RBC and matching blood types of patients. This allows clinics to use their resources efficiently and reduces the pressure on donors of Group O RhD negative blood [11]. This feature was prototyped using synthetic images only and requires validation.

Table 1. Comparison of RegenaCare with current technologies.

Representative Technologies	Sensing Modalities	Communication Methods	Power Requirements	Material Properties	Cost	Demonstrated Validation Methods	Ref.
RegenaCare	Colourimetric pH indicator (roselle, qualitative); heart rate and SpO2 (MAX30100, optical); blood type by smartphone photo (trauma version only)	NFC to a smartphone app	Battery-free, NFC energy harvesting with a capacitor (power output: 2.27–3.33 V)	PVA–gelatin–aloe vera–roselle hydrogel; tensile strength 4.91–6.34 MPa (single specimen); swelling ratio about 2.9–6.1 at 5 h; PVC outer layer	RM 154.50 (total spent); est. RM51.50 per unit	Lab-scale only (swelling, tensile, FTIR, pH colour tests); no clinical or in vivo testing, and the electronics are not validated	-
Smart Bandage for Monitoring and Treatment of Chronic Wounds by Mostafalu et al.	pH sensor (Carbon/polyaniline (PANI) and silver/silver chloride electrodes); temperature sensor; microheater (20 Ω); thermo-responsive drug carriers	Connects to computers and smartphones with wireless Bluetooth low energy module	Arduino microcontroller; power output: N/A	Alginate hydrogel sheet with PNIPAM particles	Low cost, amount: N/A	Lab-scale only (pH characterization, zone of inhibition (ZOI), number of colony-forming units (CFU) tests, bioreactor for pH calibration, bacterial study, scratch wound healing assay and cell studies), electronic validation for pH: −50 mV pH^{-1}	[3]
Flexible and Transparent pH Monitoring System with NFC for Wound Monitoring Applications by Rahimi et al.	pH sensor (direct laser scribing of indium tin oxide (ITO) films)	Reusable wireless (13.5 MHz, NFC) data transmitting platform (within 4 cm proximity)	Battery-less magnetic induction; power output: N/A	N/A	Low cost, amount: N/A	Electronic validation for pH: −55 mV pH^{-1}	[6]

Table 1. *Cont.*

Representative Technologies	Sensing Modalities	Communication Methods	Power Requirements	Material Properties	Cost	Demonstrated Validation Methods	Ref.
Battery-Free and Wireless Smart Wound Dressing for Wound Infection Monitoring and Electrically Controlled On-Demand Drug Delivery by Xu et al.	Drug delivery module	Wireless via NFC,	Battery-free; power output: higher than 2.7 V	Polypyrrole (PPy) membrane with double-layer patch dressing (top layer: reusable NFC-enabled flexible circuit board; bottom layer: disposable stretchable electrode array)	Low cost, amount: N/A	In vitro assessment of the sensors for wound monitoring, in vitro characterizations of the Electro-Responsive Drug Delivery Module, in vitro characterizations of the Electro-Responsive Drug Delivery Module, in vitro evaluation of the antibacterial efficiency of the Drug Delivery Electrode, in situ animal studies with the Smart Wound Dressing	[12]
A Highly Stretchable Smart Dressing for Wound Infection Monitoring and Treatment by Su et al.	Temperature and pH sensor; electrically controlled drug delivery system;	N/A	N/A	Ecoflex-based substrate, soft integrated circuit layer, and an ultra-thin encapsulation layer; good stretchability and long-term stable conductivity with a resistance change rate of less than 6% under 50% strain	N/A	Animal testing, antibacterial activity evaluation, in vitro biocompatibility assessment	[8]

Despite this progress, most smart wound dressing research addresses sensing, data processing, or communication in isolation, with limited integration into a single low-cost platform connected to a complete healthcare workflow. This paper presents RegenaCare, a smart bandage that combines a PVA-based hydrogel membrane for wound contact, an NFC-enabled electronic subsystem and a companion mobile application. It is an integrated prototype for preliminary colourimetric monitoring and physiological sensing, with potential application to patients with diabetic ulcers and trauma wounds. By leveraging near-field communication for wireless power harvesting and data transmission, this system facilitates a prototype framework for integrating wound-related sensing with NFC that minimizes the need for cumbersome external power supplies [12]. In this paper, the project aims to develop a PVA-based hydrogel membrane for wound-contact applications, integrated with a web-hosted monitoring interface to support patient and clinician access to sensor data. The main contributions and innovations of this work are the addition of a blood-typing feature and hibiscus extract for pH sensing into the smart bandage, which were all demonstrated to have feasibility.

2. Results

The membranes produced had varying textures depending on the drying method chosen. Hydrogels that underwent freeze–thawing and freeze-drying formed a more foam-like and porous texture. On the other hand, hydrogels that went through oven-drying resulted in a less porous, denser film matrix. Figure 1 shows the result of the hydrogel formulations while Figure 2 show the final product with the integrated electronics.



Figure 1. Photographs of fabricated hydrogel membrane samples. From left to right: freeze-dried membrane no gelatin, freeze-dried membrane 1.5 g gelatin, oven-dried 1.5 g gelatin, oven-dry no gelatin.

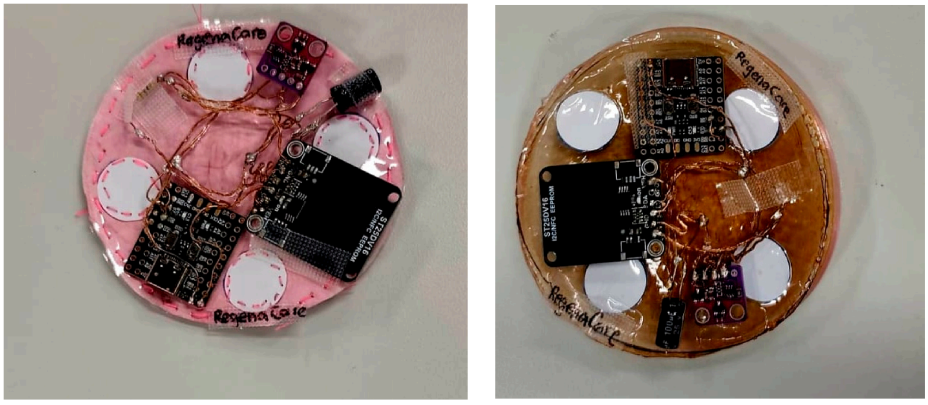

(**a**) (**b**)

Figure 2. Prototype. (**a**) 1.5 g gelatin freeze-dried (**b**) 1.5 g gelatin oven-dried.

2.1. Swelling Behaviour

Table 2 shows the results of the hydrogel swelling test, which is plotted in Figure 3.

Table 2. Swelling ratio of membranes without roselle extract.

Formulation	Hour 0	Hour 1	Hour 2	Hour 3	Hour 4	Hour 5
Oven-dry, Aloe vera only	1	2.73	2.64	2.45	2.45	2.36
Oven-dry, Gelatin only	1	5.73	5.45	5.27	5.27	5.18
Oven-dry, Aloe vera + Gelatin	1	7.40	7.00	7.10	6.80	6.50
Freeze-dry, Aloe vera + Gelatin	1	7.37	9.42	8.21	7.89	7.74

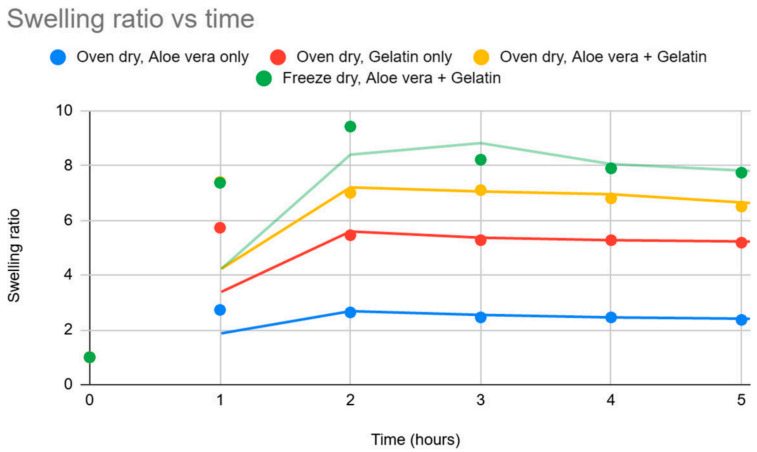

Figure 3. Swelling ratio over time for membranes without roselle extract.

Upon testing the non-roselle containing samples, the samples containing the roselle extract were tested, with results in Table 3 and plotted in Figure 4, where n shows the number of repetitions.

Table 3. Swelling ratio of membranes with roselle extract, mean ± SD (n = 3).

Formulation	Hour 1	Hour 2	Hour 3	Hour 4	Hour 5
Oven-Dry, No Gelatin	2.64 ± 0.60	3.35 ± 0.37	3.09 ± 0.87	3.44 ± 0.86	4.12 ± 0.82
Oven-Dry, 1.5 g Gelatin	3.33 ± 1.07	2.95 ± 0.78	2.88 ± 0.90	2.68 ± 0.80	2.86 ± 0.61
Freeze-Dry, No Gelatin	6.11 ± 0.32	5.82 ± 0.20	6.23 ± 0.74	6.14 ± 0.35	6.14 ± 0.47
Freeze-Dry, 1.5 g Gelatin	4.85 ± 0.23	5.03 ± 0.23	5.21 ± 0.31	5.49 ± 0.29	5.42 ± 0.21

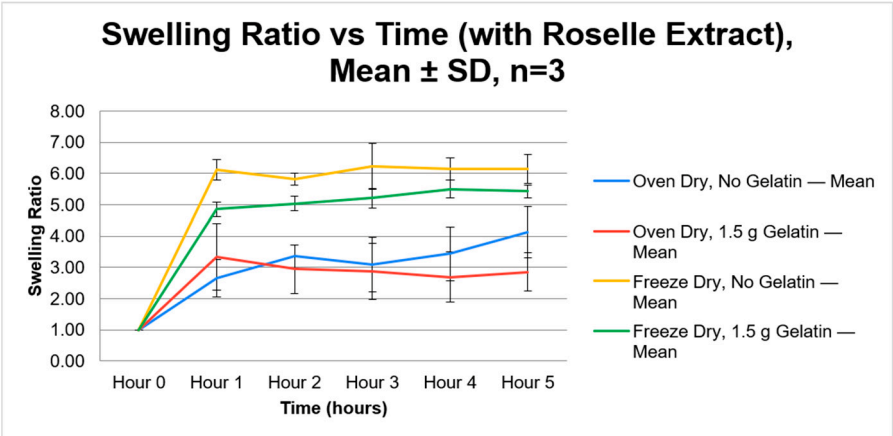

Figure 4. Swelling ratio over time for membranes with roselle extract, mean ± SD (n = 3).

2.2. Tensile/Mechanical Properties

Tensile properties were obtained from a single specimen per formulation (refer to Section 4.5.2); the values below should therefore be interpreted as indicative of formulation trends rather than statistically validated differences between formulations. Figures 5–8 show the tensile test results for each formulation.

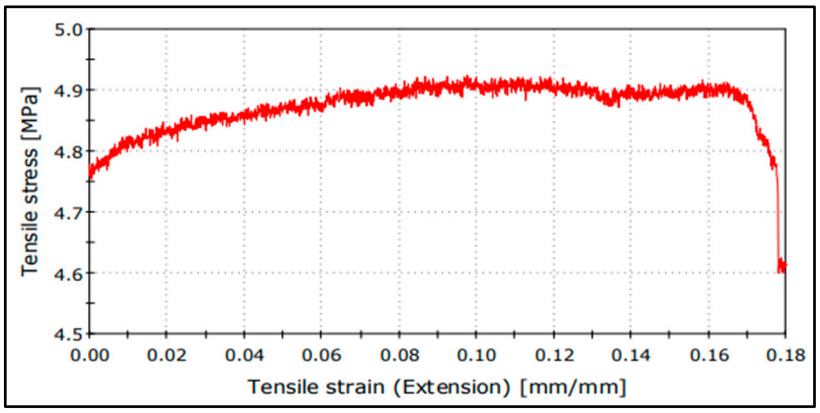

Figure 5. Freeze-dry no gelatin.

The freeze-dried sample without gelatin recorded a tensile strength of 4.91 MPa (Young's modulus 5.08 MPa). The stress–strain curve showed a gradual increase up to a peak stress of 4.9 MPa at a strain of approximately 0.10–0.16 mm/mm, with failure at a strain of 0.17 mm/mm. This is comparable to a freeze–thaw crosslinked PVA composite hydrogel reported for wound dressing applications (5.6 MPa) [13], showing that the freeze-dried PVA formulation exceeded the tensile-strength target defined for this project.

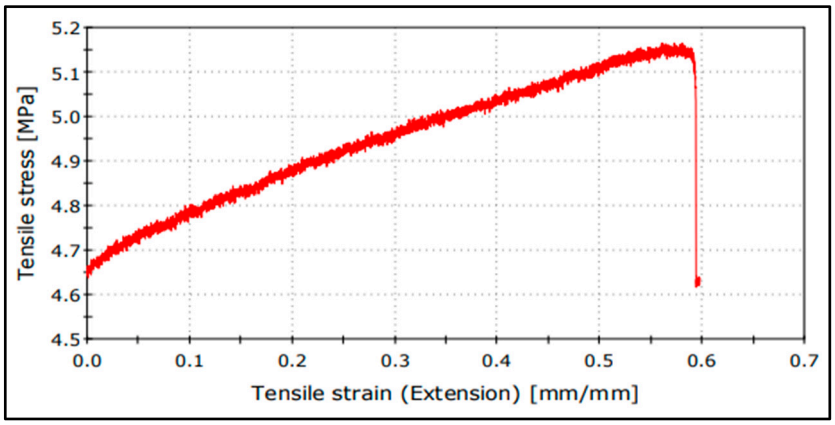

Figure 6. Freeze-dry 1.5 gelatin.

Adding 1.5 g gelatin to the freeze-dried sample increased both tensile strength (5.15 MPa) and strain at break (0.6 mm/mm vs. 0.17 mm/mm), indicating an improved flexibility and elongation capacity consistent with gelatin's established role as a flexibility-enhancing agent [13].

The oven-dried sample without gelatin achieved a higher tensile strength of 5.96 MPa, exceeding the freeze–thaw PVA benchmark [13] and suggesting that oven-drying produces a denser, more tightly packed PVA network.

The oven-dried sample reinforced with 1.5 g gelatin achieved the highest tensile strength recorded across all formulations (6.3–6.34 MPa) at the greatest elongation. The

single tested oven-dried, gelatin-reinforced specimen had the highest tensile strength among the tested specimens.

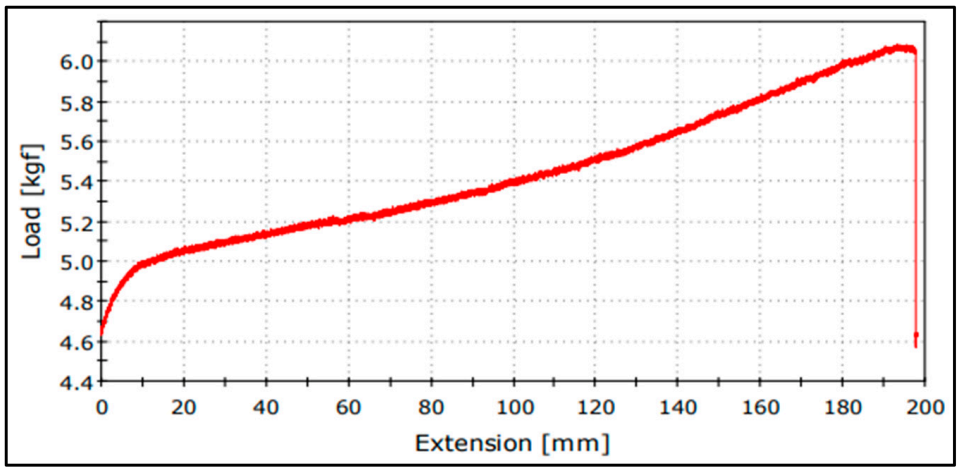

Figure 7. Oven-dry no gelatin.

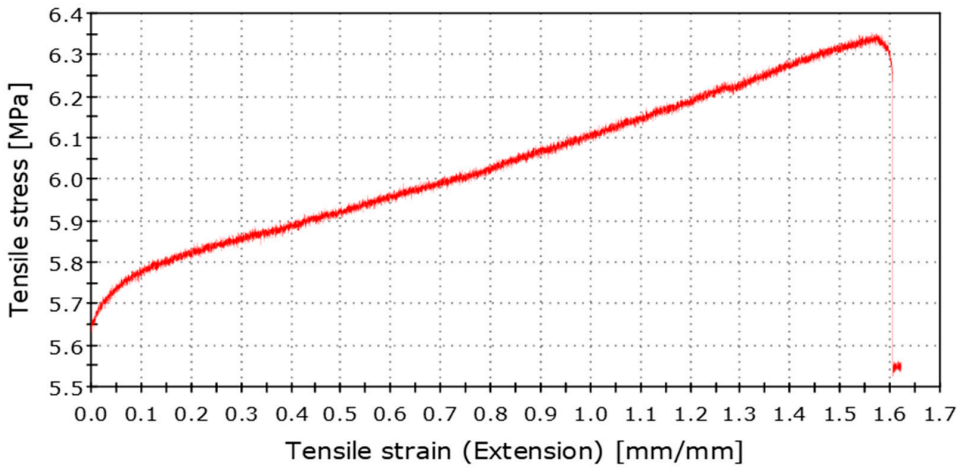

Figure 8. Oven-dry 1.5 gelatin.

Due to failure of the automatic calculation in the UTM Bluehill 3 software for the gelatin-containing samples, their Young's modulus was estimated manually from the raw data, using the same region of the stress–strain curve that the software used for the corresponding gelatin-free sample (the initial region for the freeze-dried samples and the long linear region for the oven-dried samples). The values are therefore comparable between gelatin-free and gelatin-containing samples within the same drying method, but not directly between drying methods. The values of the Young's modulus obtained (approximated values) are shown in Table 4.

Table 4. Approximate values of Young's modulus obtained.

Formulation	Young's Modulus (MPa)
Oven-Dry, No Gelatin	0.787
Oven-Dry, 1.5 g Gelatin	0.4
Freeze-Dry, No Gelatin	5.08
Freeze-Dry, 1.5 g Gelatin	2.6

2.3. FTIR Characteristics

Figures 9–17 show the results of the FTIR, with the main peaks' (O–H bond) positions and transmittance values tabulated in Table 5.

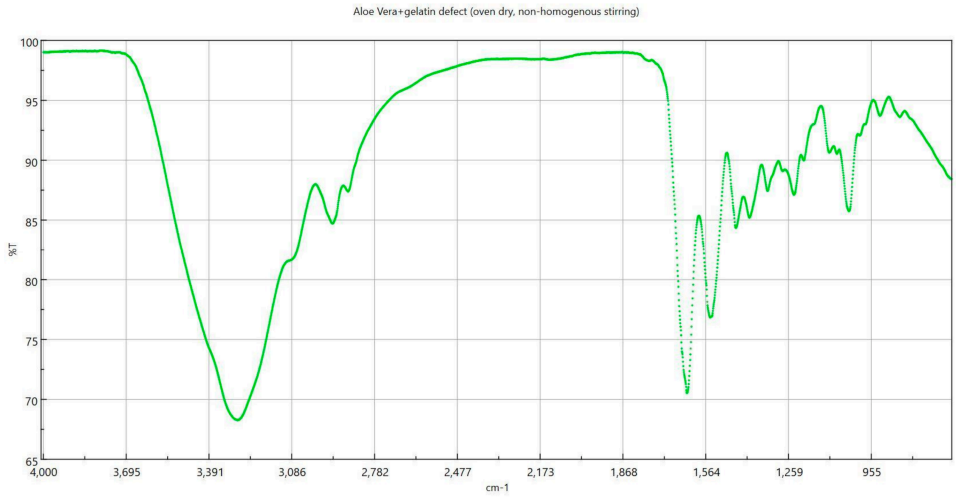

Figure 9. Aloe vera + Gelatin defective (oven-dry, non-homogeneous stirring).

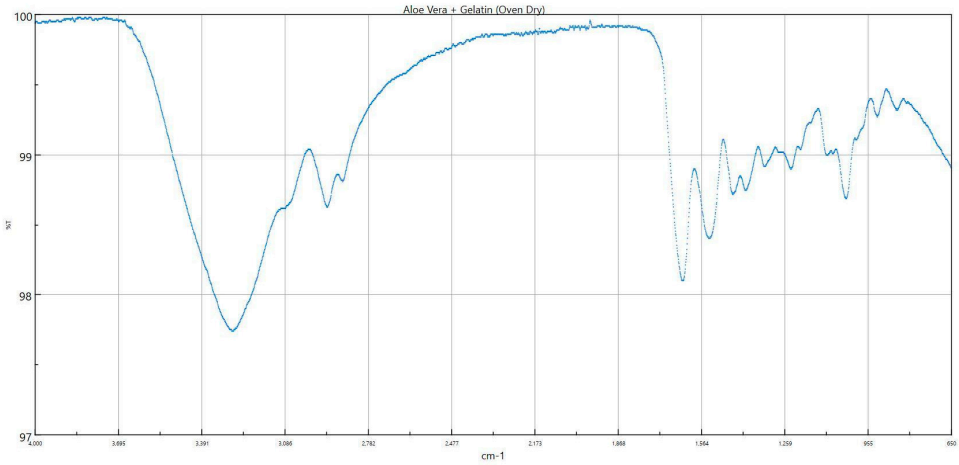

Figure 10. Aloe vera + Gelatin (Oven-dry).

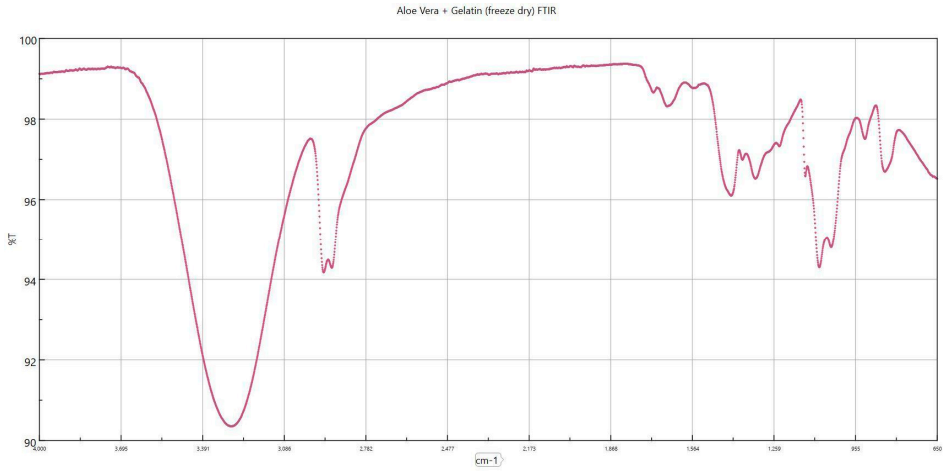

Figure 11. Aloe vera + Gelatin (freeze-dry).

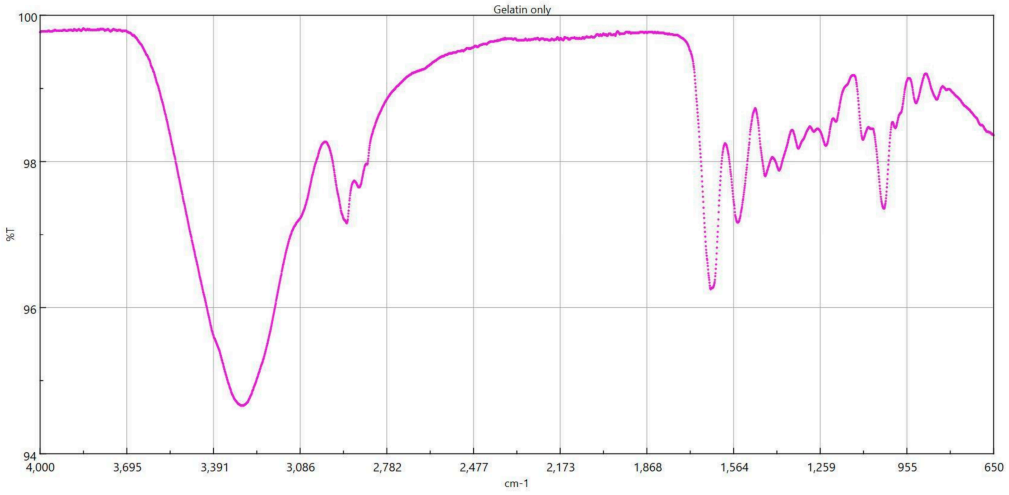

Figure 12. Gelatin only.

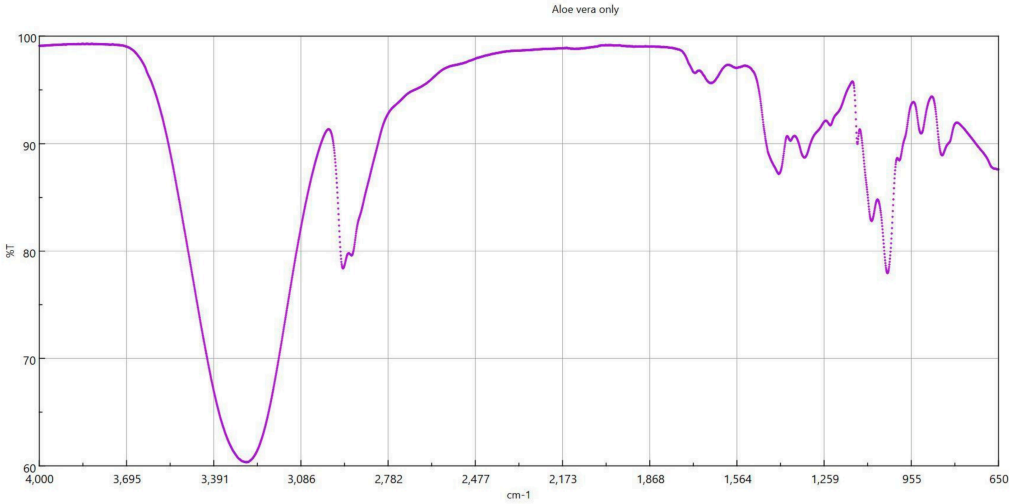

Figure 13. Aloe vera only.

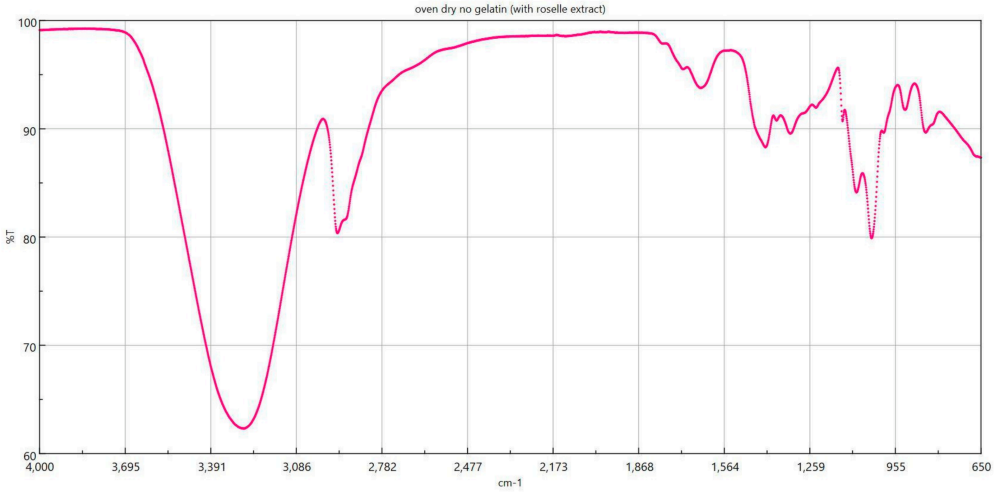

Figure 14. Oven-dry no gelatin with roselle extract.

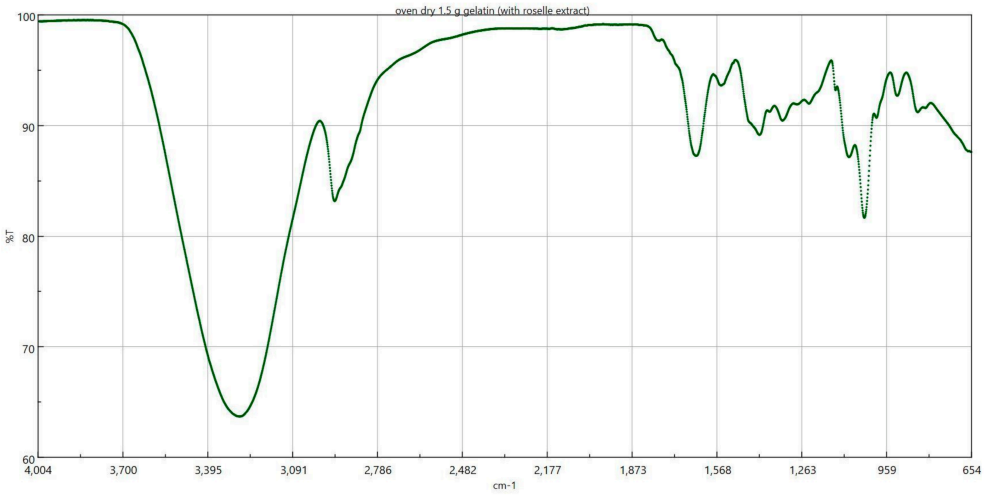

Figure 15. Oven-dry 1.5 g gelatin with roselle extract.

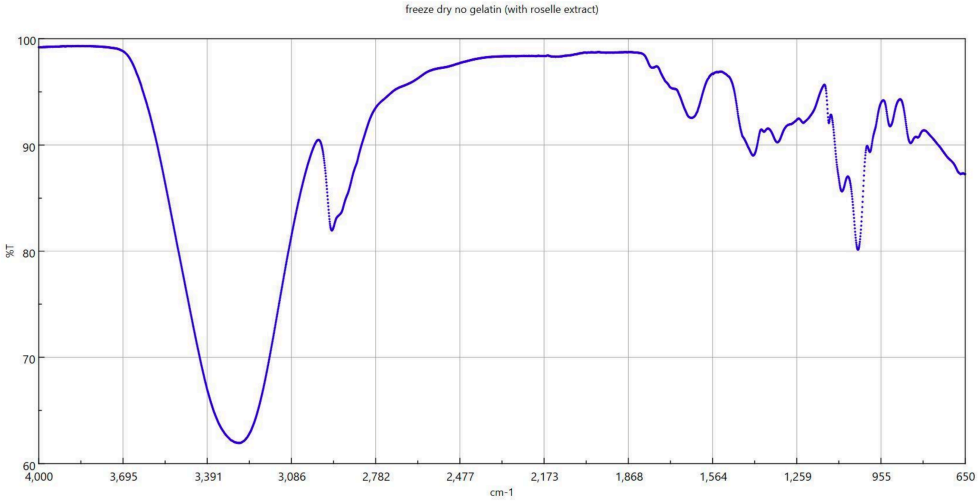

Figure 16. Freeze-dry no gelatin with roselle extract.

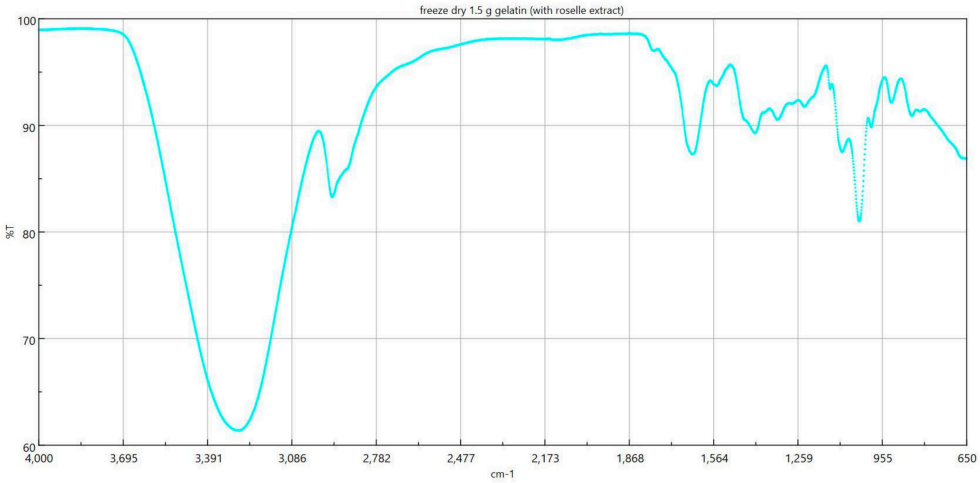

Figure 17. Freeze-dry 1.5 gelatin with roselle extract.

Table 5. FTIR O–H bond.

Formulation	O–H Bond Peak (cm^{-1})	Transmittant (%T)
Oven-dry, Aloe Vera only	3277.33	60.34
Oven-Dry, Aloe vera + Gelatin (defect)	3286.41	68.1
Oven-Dry, Aloe vera + Gelatin (homogenous)	3278.71	97.74
Oven-Dry, Gelatin only	3287.26	94.66
Freeze-Dry, Aloe vera + Gelatin	3282.82	90.35
Oven-Dry, No Gelatin (with roselle)	3274	62.31
Oven-Dry, 1.5 g Gelatin (with roselle)	3281	63.37
Freeze-Dry, No Gelatin (with roselle)	3280	61.94
Freeze-Dry, 1.5 g Gelatin (with roselle)	3279	61.37

2.4. Colour Change

2.4.1. pH Solution Colour Change

The colour change of the roselle extract are shown in Figure 18 (range of wound pH: pH 6, 6.5, 7, 7.5, 8) and Figure 19 (extreme pH: pH 1 and 11).

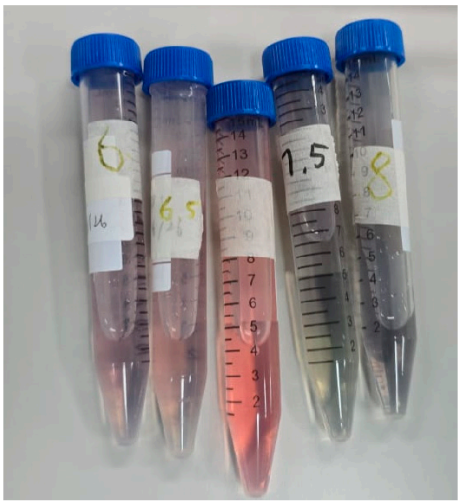

Figure 18. Roselle hibiscus extract colour change across pH 6–8.

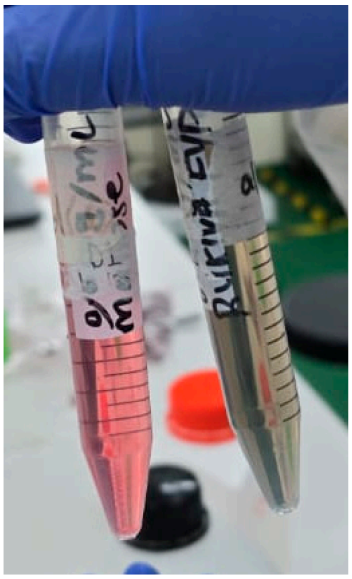

Figure 19. Roselle hibiscus extract colour change at pH 1 and pH 11.

2.4.2. Smart Bandage Colour Change

Once the roselle extract solution was tested, the hydrogels with the incorporated roselle extract were tested on the observe the colour change, as shown in Figures 20–22.

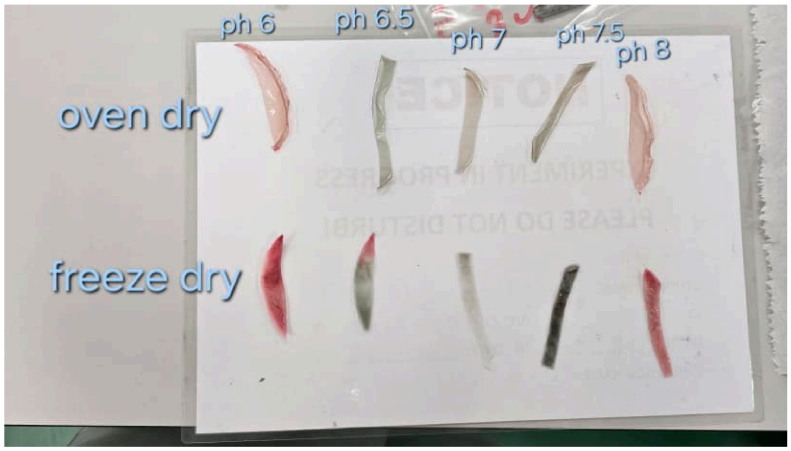

Figure 20. Smart bandage hydrogel colour change across pH 6–8. (**Top**): Oven-dried no gelatin. (**Bottom**): Freeze-dried 1.5 g gelatin.

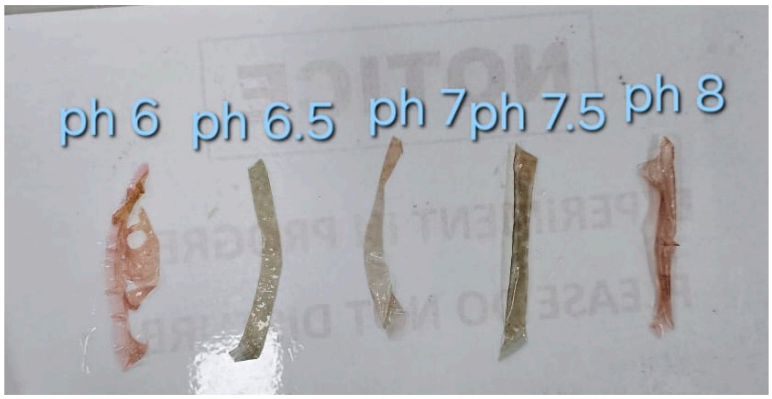

Figure 21. Smart bandage hydrogel colour change across pH 6–8. Oven-dried 1.5 g gelatin.

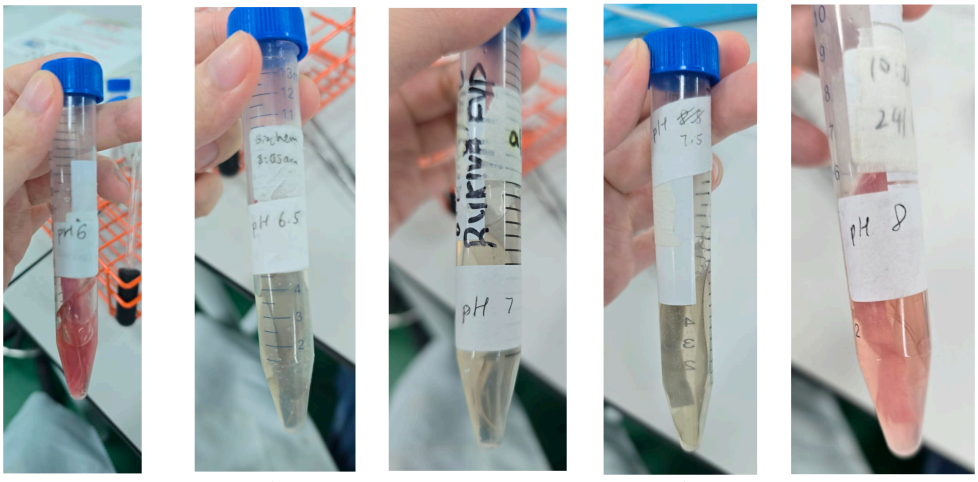

(**a**) (**b**) (**c**) (**d**) (**e**)

Figure 22. Smart bandage colour progression from pH 6 to 8. (**a**) pH 6 (**b**) pH 6.5 (**c**) pH 7 (**d**) pH 7.5 (**e**) pH 8.

2.4.3. UV-Vis Data

Figures 23–29 show the results for the UV-Vis spectrum of the pH colour changes.

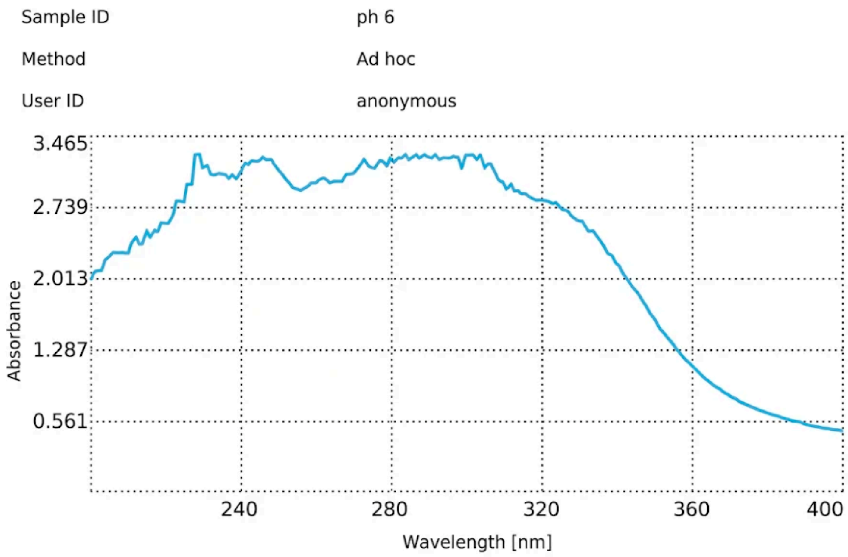

Figure 23. UV-Vis spectrum at pH 6.

For pH 6, the UV-Vis spectrum had a high absorbance of 3.3 A when the wavelength was approximately 229 nm, as well as from 284 to 302 nm. Between 212 and 302 nm, the absorbance showed fluctuations within the range of 2.398 to 3.3 A absorbance values, before decreasing at wavelengths above 302 nm, achieving an absorbance value less than 0.561 A at 400 nm.

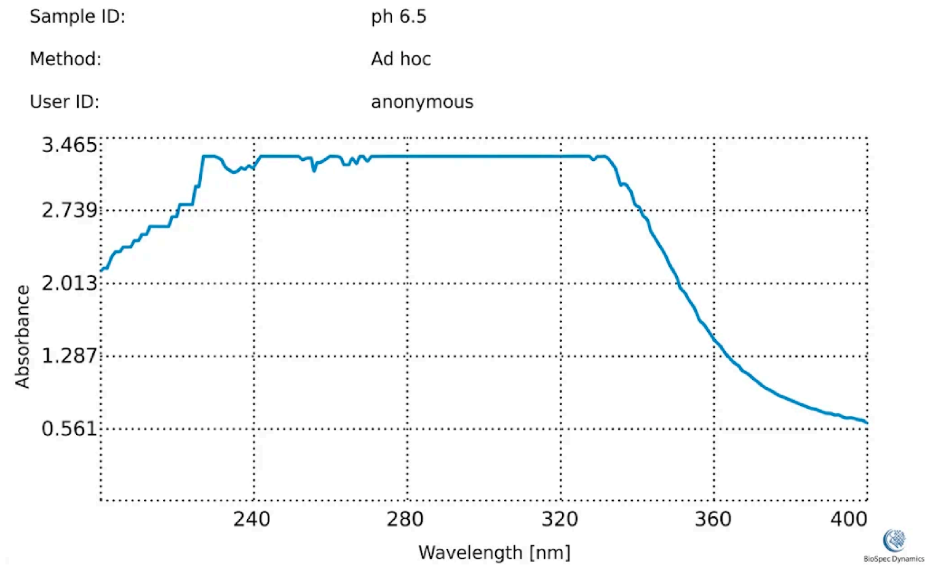

Figure 24. UV-Vis spectrum at pH 6.5.

The UV-Vis spectrum of the sample at pH 6.5 showed high absorbance in the wavelength range of approximately 229–332 nm. The spectrum exhibited apparent absorption maxima at 229, 254, 262 and 332 nm, with absorbance values of approximately 3.30. The absorbance subsequently decreased at wavelengths above 330 nm, reaching approximately 0.56 at 400 nm.

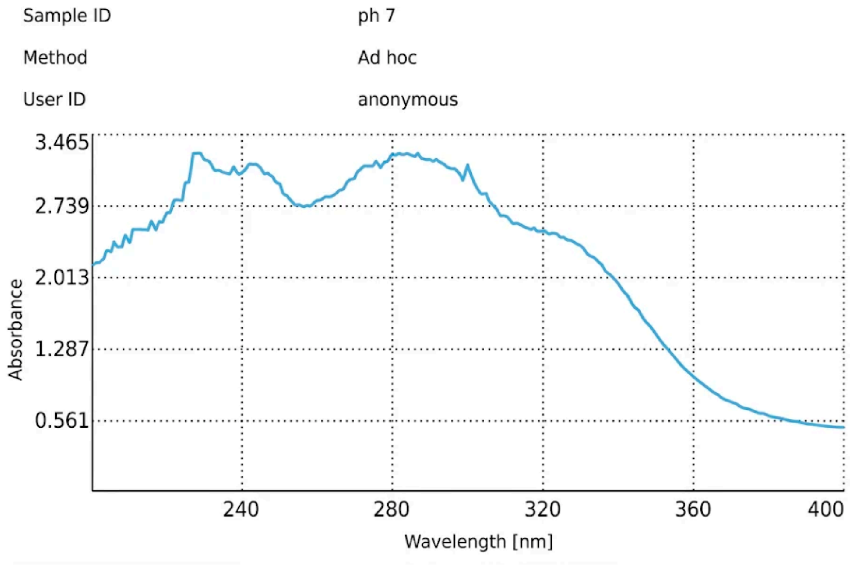

Figure 25. UV-Vis spectrum at pH 7.

The UV-Vis spectrum of the sample at pH 7 showed higher absorbance within 2.398–3.3 A in the wavelength range of 206–300 nm. The absorbance value peaked at a wavelength of 229 nm with 3.3 A, before declining to 3.154 A at 239 nm, then peaking at 3.3 A again at a wavelength of 287 nm. At wavelengths above 300 nm, the absorbance value slowly declined until a value less than 0.561 A was obtained at a wavelength of 400 nm.

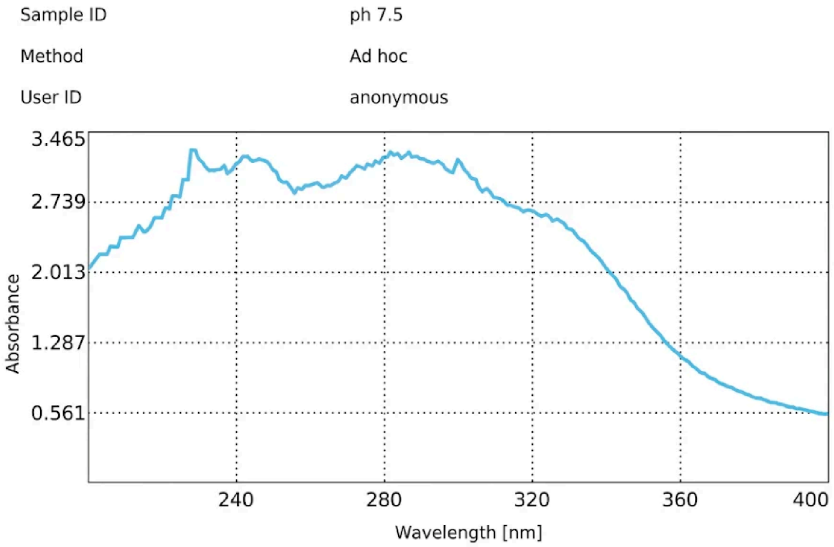

Figure 26. UV-Vis spectrum at pH 7.5.

At pH 7.5, higher absorbance values ranging from 2.456 to 3.3 A were observed in the wavelength range of 214–300 nm. The absorbance value peaked at a wavelength of 229 nm with 3.3 A, while the lowest absorbance value was 2.456 A at 216 nm. At wavelengths above 300 nm, the absorbance value slowly declined until a value less than 0.561 A was obtained at a wavelength of 400 nm.

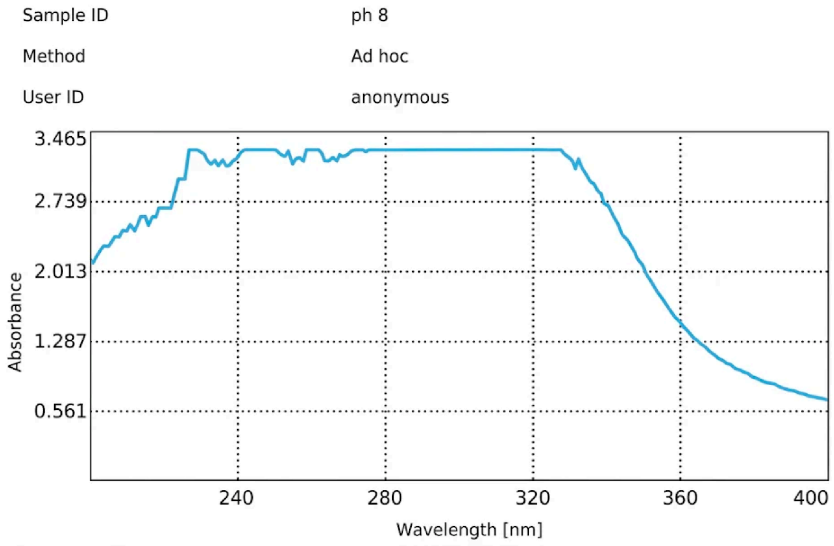

Figure 27. UV-Vis spectrum at pH 8.

At pH 8, the absorbance values were higher at wavelengths of 211–333 nm. From 211 to 262 nm, the absorbance values showed fluctuations ranging from 2.523 to 3.3 A. From 262 to 328 nm, the absorbance remained constant at 3.3 A, before declining to 3.199 A at 333 nm and achieving an absorbance just over 0.561 A at 400 nm.

In order to directly compare the UV-Vis data at extreme pH ranges, the data obtained at pH 1 and 11 were compared. At pH 1, higher absorbance values were observed at wavelengths 231–300 nm; at pH 11, higher absorbance values were observed at wavelengths 210–310 nm. At pH 1, the highest absorbance value was 3.3 A, and from 231 to 300 nm, the absorbance value showed fluctuations ranging from 2.870 to 3.3 A, where the absorbance value dropped from 3.3 A to 2.870 A from wavelengths 243 to 258 nm, before increasing to 3.266 A at 297 nm. The absorbance then decreased until 0.561 A was achieved at 400 nm. In contrast, for pH 11, while there were minor fluctuations in absorbance value ranging from 2.523 to 3.3 A from wavelengths 210 to 238 nm, the absorbance remained constant from 238 to 309 nm, before gradually decreasing to a value of more than 1.287 A at 400 nm.

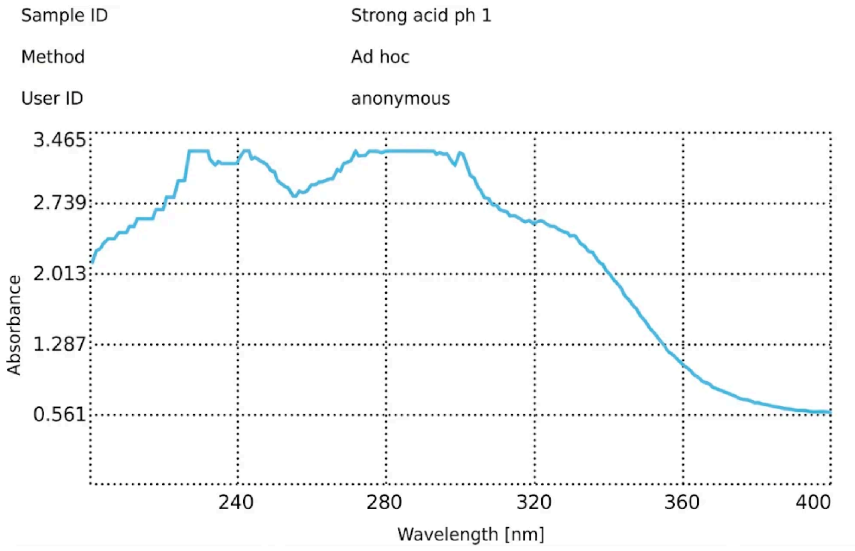

Figure 28. UV-Vis spectrum at pH 1.

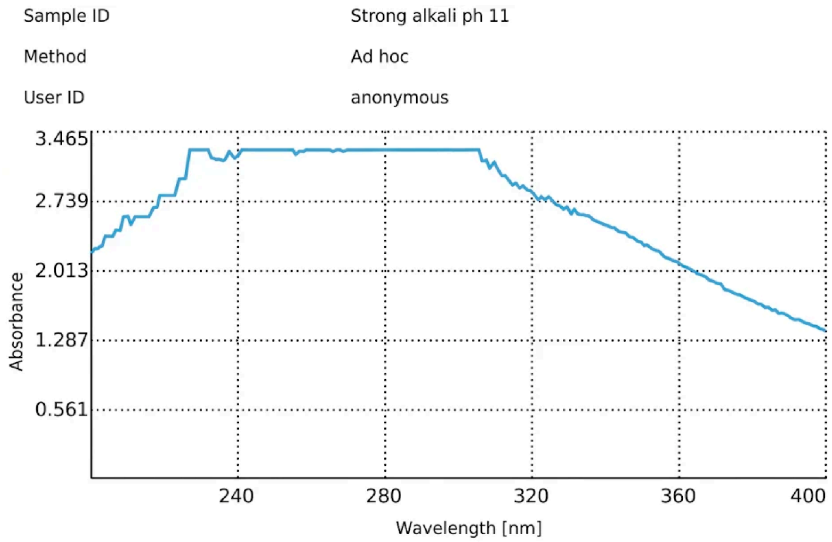

Figure 29. UV-Vis spectrum at pH 11.

2.5. Electronics

The power output of the NFC energy harvested was tested to be approximately 2.27 to 3.33 V, as shown in the schematization and results in Figure 30.

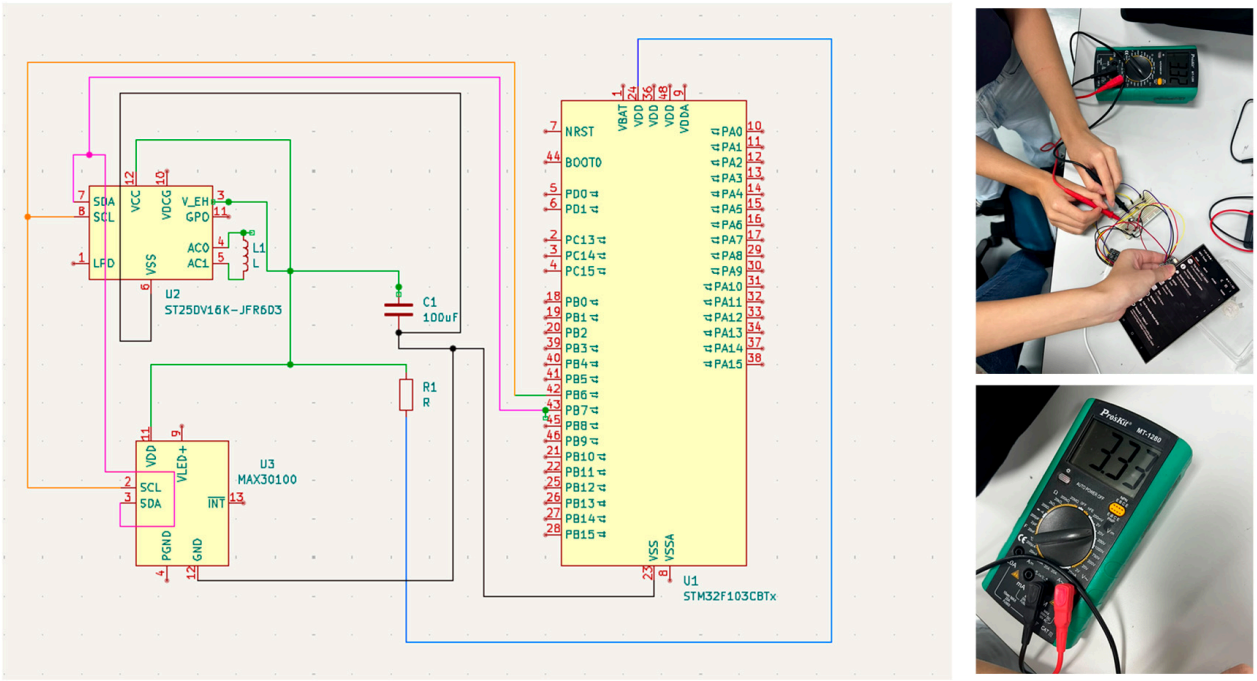

Figure 30. Schematic of Electronic components with multimeter readings.

Upon testing, the capacitor charging time was measured to be approximately 5 to 8 s. However, to obtain more accurate results for the blood-flow rate, a charging time of approximately 35 s is needed. For the reading range, the phone needs to be placed directly on top of the NFC tag to charge the circuit.

3. Discussion

3.1. Swelling Behaviour

During formulation trials, freeze-dried aloe vera + gelatin samples showed the highest swelling ratio (7.37–9.42), followed by oven-dried aloe vera + gelatin (7.00–7.40); gelatin-only and aloe vera-only samples showed lower ratios (2.36–5.73). These preliminary trials were conducted as single runs to identify the optimal formulation and are not reported with variance. All formulations reached equilibrium by two hours.

For the final roselle-incorporated formulation, three replicate specimens were tested per condition ($n = 3$). Freeze-dried samples without gelatin showed the highest swelling ratio, reaching 6.23 ± 0.74 at 3 h and stabilizing at 6.14 ± 0.47 by 5 h, followed by freeze-dried samples with 1.5 g gelatin (5.42 ± 0.21 at 5 h). Oven-dried samples showed lower and more variable swelling: the gelatin-free oven-dried formulation reached 4.12 ± 0.82 at 5 h, while the gelatin-reinforced oven-dried formulation showed the lowest and most variable swelling ratio (2.86 ± 0.61 at 5 h). Across all four formulations, the addition of 1.5 g gelatin reduced both the mean swelling ratio and, in most cases, its variability relative to the gelatin-free equivalent, consistent with gelatin forming a denser polymer network that restricts water penetration despite being intrinsically hydrophilic. The relatively large standard deviations observed in the oven-dried formulations (up to ± 1.07) indicate greater specimen-to-specimen variability in this drying method compared to freeze-drying, which may reflect less uniform moisture removal during oven-drying. Their swelling was measured in water so that the four formulations could be compared under the same simple conditions. The absolute swelling ratios in wound exudate, which contain salts and proteins, may differ from those reported here, and testing in PBS or simulated wound fluid is needed and may be considered for future development.

3.2. Tensile/Mechanical Properties

All formulations exceeded the design target tensile strength range of 0.5–1.5 MPa specified in the project objectives, which was the project's tensile-strength target. Since human skin has a lower modulus than the smart bandage, and considering that the human skin stretches to around 30% strain during body movement, the tensile strength of this formulation needs to be lowered before it can be used. Besides hydrogel, the electronics also need to be able to blend with the skin without sacrificing performance quality [8]. This is to ensure that the bandage can stretch together with the skin. If the hydrogel's tensile strength is too high, it may indicate that it is too rigid. This can cause it to pull against and cause excessive shear stress on the skin. Tension should be situated away from the skin edge to help reduce wound injury, pain and discomfort, as well as improve recovery [14].

In this case, tensile testing can be considered as a screening step to determine whether the candidate (membranes) met the design target. All formulations (4.91–6.34 MPa) exceeded the 0.5–1.5 MPa target by a wide margin, so this conclusion does not depend on small differences between formulations. Since the formulations substantially surpassed the ideal tensile strength, the formulations should be further optimized before doing tensile testing again with five replicates to determine reproducibility. The five replicates are needed to evaluate and determine the average tensile strength across the whole hydrogel, and make sure all parts are consistently similar to the 0.5–1.5 MPa instead of having different areas of the hydrogel have significant differences in tensile strength, which can lead to tension in the wound area and disrupt healing.

Aside from tensile strength, another parameter that can be studied is the Young's modulus. Young's modulus is a mechanical property that measures the stiffness of a solid material under tension or compression. A higher Young's modulus would mean that the material is stiff. Hence, tensile strength shows the strength of the material, while the Young's

modulus shows its stiffness. The Young's modulus obtained showed that the freeze-dried membrane is stiffer than the oven-dried samples, and that gelatin-containing samples were stiffer than samples without gelatin. Indentation tests done by Kalra et al. show that the Young's modulus in the thickness-direction is between 5 and 100 kPa, while tensile test values are between 25 kPa and 140 MPa. The skin is viscoelastic because the higher the strain rate, the higher the Young's modulus. Different areas of the body and age may also affect the Young's modulus. For example, the back area of 81–97-year-old subjects may have a mean Young's modulus of approximately 83.33 ± 4.9 MPa, while human skin on the calf can have maximum and minimum values of Young's modulus of 0.32 and 4 MPa respectively, and 0.3 and 20 MPa across the tibial axis [15,16]. Hence, future development may need to consider smart bandages of different Young's modulus for different parts of the body alongside developing a measure of testing for viscoelastic behaviour, flexibility, tear resistance, and adhesion.

3.3. FTIR Characteristics

All samples exhibited characteristic broad O–H stretching bands near 3200–3300 cm^{-1}, together with amide I (~1650 cm^{-1}) and amide II (~1550 cm^{-1}) peaks confirming gelatin's protein backbone in gelatin-containing formulations; these amide bands were absent in the no-gelatin samples, confirming the absence of a protein component. This is because PVA contains no N–H groups. There were no new bands observed in the formulations with roselle extracts, which indicates the components were physically blended through hydrogen bonding rather than chemically bonded, although the overlap of hydroxyl-related bands limits how firmly this can be stated. The O–H band position showed little variations between formulations (3274–3287 cm^{-1}), with differences of only a few cm^{-1}. This indicates that the hydroxyl-related hydrogen bonding is considered to be broadly similar across the membranes.

The stretching bands at 3200–3300 cm^{-1} is consistent with the hydroxyl-rich nature of the hydrogel components, particularly PVA, aloe vera and glycerol. Pure PVA commonly shows a broad O–H stretching band around 3273–3300 cm^{-1} due to intermolecular and intramolecular hydrogen bonding, while PVA also shows C–H stretching bands near 2900–2940 cm^{-1} and C–O-related bands in the fingerprint region [16,17]. Therefore, the broad O–H band observed in the present formulations is likely due to the overlapping contributions of the hydroxyl groups from PVA and the other components. Glycerol may also contribute to the broad O–H absorption region because it contains three hydroxyl groups. Pure glycerol has reported C–H stretching bands near 2931 and 2879 cm^{-1} and a characteristic C–O stretching region around 1045–1050 cm^{-1} [16,18]. All formulations have the C–H stretching band so it confirms the organic backbone but cannot distinguish between them. In PVA-based materials, glycerol can form hydrogen bonds with PVA, potentially affecting the shape and intensity of the O–H absorption band. However, because glycerol, PVA and aloe vera have overlapping hydroxyl-related absorption bands, the contribution of glycerol cannot be clearly separated in the composite FTIR spectra.

The defective sample fabricated with non-homogeneous stirring showed a deeper, broader O–H trough and a sharper amide dip than the homogeneous oven-dry sample, consistent with the uneven material distribution observed during fabrication. Across all the roselle-incorporated formulations, transmittance values were generally lower than in samples without roselle extract, indicating that the extract contributes additional infrared absorption in the fingerprint region. The drying method (oven-dry and freeze-dry) did not noticeably shift peak positions between non-defective samples, indicating that it primarily affects the physical structure of the membrane rather than its chemical composition. The defective sample prepared under non-homogeneous stirring showed a deeper and broader

O–H absorption band and a sharper amide absorption compared with the homogeneous oven-dried sample. This difference may be caused by uneven distributions of the hydroxyl-rich and gelatin components, resulting in local differences in hydrogen bonding and material concentration. However, the overall peak positions remained similar, suggesting that the defect mainly affected the physical distribution of the components rather than introducing major chemical changes.

The gelatin-containing formulations showed more distinct absorption bands around 1650 cm^{-1} and 1550 cm^{-1}, corresponding to the characteristic amide I and amide II regions of gelatin, respectively. These values agree with previous studies reporting gelatin amide I bands around 1634–1655 cm^{-1} and amide II bands around 1550 cm^{-1} [18,19]. In contrast, the no-gelatin samples lacked the same distinct amide II absorption around 1550 cm^{-1}. Although PVA may exhibit absorption near 1650 cm^{-1} due to absorbed water or overlapping vibrations, the simultaneous presence of bands around 1650 and 1550 cm^{-1} provides a stronger evidence of gelatin incorporation.

The aloe vera-only sample showed a broad O–H absorption band at approximately 3277.33 cm^{-1} and a smaller absorption band near 2900 cm^{-1}. These findings are consistent with published PVA/aloe vera hydrogel studies, which reported broad O–H absorption around 3253–3300 cm^{-1} and C–H stretching near 2925–2941 cm^{-1} [20,21]. Since both PVA and aloe vera contain hydroxyl groups, their absorption bands overlap in the composite formulation, contributing to the broad O–H region.

The oven-dried and freeze-dried non-defective samples showed no major shift in the principal absorption bands. The O–H region remained around 3200–3300 cm^{-1}, while gelatin-containing samples retained the characteristic amide I and amide II bands. This suggests that the drying method did not substantially alter the main chemical functional groups of the hydrogel. The observed differences in peak intensity and band shape are more likely to be related to changes in moisture content, hydrogen bonding and physical structure.

Across all four roselle-incorporated formulations, %T values were generally lower compared to samples without roselle extract, indicating that the roselle extract absorbs more infrared radiation, contributing additional peaks in the fingerprint region and altering the overall transmittance profile of the hydrogel. All four samples retained the characteristic broad O-H band at around 3200–3300 cm^{-1}. The gelatin-containing samples showed more clearly defined amide I and amide II peaks (1650–1550 cm^{-1}), supporting the presence of gelatin-associated amide bands regardless of drying method, while the no-gelatin samples lacked these distinct amide bands. Drying method (oven vs. freeze) did not significantly alter peak positions, suggesting it affects physical structure more than chemical composition. Table 6 shows a comparison between band positions in RegenaCare with literature values.

Table 6. Comparison with literature values.

Type of Band	RegenaCare (cm^{-1})	Literature Value (cm^{-1})	Ref.
O–H band	3274–3287.26	3200–3300 Pure PVA: 3273–3300	[16,17]
O–H stretching, PVA/aloe vera hydrogels	3277.33 (aloe vera only)	3253–3300	[20,21]
C–H stretching, PVA	2922.7–2939.48	2900–2940	[16,17]
C–H stretching (aloe vera only)	2939.39	2925–2941	[20,21]
Amide I (gelatin-containing samples)	1632.62–1643.94	1634–1655	[18,19]
Amide II (gelatin-containing samples)	approximately 1550	about 1550	[18,19]

3.4. Colour Change

3.4.1. pH Solution Colour Change

Generally, for pH solutions, the colour change observed followed the following trend: redness that gradually fades at acidic ranges (pH 1, 6, 6.5), pink at neutral (pH 7), and green or violet colours at alkaline ranges (pH 7.5, 8, 11). The slight inconsistency is due to the stability of the anthocyanins. Theoretically, the colour change should occur as follows: below 3, the pH indicator appears red, and from pH 4 to 6, the pH indicator's red colour should fade. At pH 7 to 9, the structure gradually turns colourless and the anthocyanins gradually turn blue. Lastly, at pH 9 and above, the colour of the pH indicator should have changed from red to yellowish green as the anthocyanins are decomposed [22]. The reason the results obtained differ slightly from the literature is due to pH, temperature, light and storage affecting their stability. Anthocyanins are relatively unstable. Due to this, the anthocyanins can degrade quickly. Their high reactivity forms colourless or brown compounds during extraction and storage which are undesired. Additionally, as pH increases, the anthocyanins undergo destruction, so it is more unstable in alkaline pH ranges compared to acidic pH ranges [23].

3.4.2. Smart Bandage Colour Change

From the images, within the targeted pH range of 6–8, the hydrogel exhibited a non-monotonic qualitative colour response across the tested pH range, changing from pink at pH 6, to green at pH 6.5, white at pH 7, green at pH 7.5 and pink at pH 8. Since the response was not progressive, the present data do not establish a quantitative pH calibration. The hydrogel's colour change differs from that in solution because of its integration into the PVA, gelatin, glycerol and aloe vera hydrogel matrix. The incorporation of roselle hibiscus extract into a hydrogel may affect the diffusion rate of H^+/OH^- through the hydrogel as hydrogels composed of gelatin and glycerine have a microstructure with a compact surface domain and porous internal network. The diffusion of H^+ and OH^- ions through the hydrogel is regulated, which causes a slower, more gradual and stable pH colour transition. Additionally, proteins such as gelatin have a binding affinity for anthocyanins. Their interactions consist of Van der Waals forces, hydrophobic interactions, and covalent and H bonding which can also slow down anthocyanin degradation. The gradual colour change is reflected in the results, when the colour change was only observed after 1 to 2 min instead of instantaneously like the solution [24–26]. Since anthocyanins can be affected by temperature, pH and solvents, these factors need to be controlled to obtain proper and relevant results on their antioxidant activity [27]. According to a study by Amperawati et al. on the anthocyanins content, colour changes and thermal stability of roselle flowers, to ensure anthocyanin stability, they should be processed and stored at low temperatures, with low availability of O_2, and avoiding light [28]. According to Wu et al. [29], anthocyanins in roselle extract have a certain degree of heat resistance and good colour stability when it is put in an acidic environment. However, they degrade quickly and show more noticeable changes when they are in extreme acid environments and is more easily affected by heat treatment in such an environment [29]. In a study by Sipahli et al. [30] on anthocyanin extracts from roselle hibiscus, after 7 days of incubation, brown precipitate was formed in samples with a pH from 6 to 9. In the same study, it was established that pH and anthocyanin structure can affect anthocyanin colour stability, and that colour change is more significant in alkaline pH due to instability. Generally, roselle extract pigments are more stable at lower pH values, especially at pH 5 to 6 because there is a general increasing trend of degradation [30]. Within the required functional range of pH 6–8, for the most part, the anthocyanins have good colour stability. However, when the pH environment becomes more alkaline, similarly to an infected wound, the pigments degrade more easily

and develop some instability, causing more colour change. Since colour changes caused by pigment degradation cannot be distinguished from those caused by pH, this instability must be resolved before the indicator can be used for infection detection.

Regarding leaching, while a denser network of hydrogel may improve the retention of the anthocyanin pigments and potentially reduce the risk of leaching, it can also cause a reduction in swelling, effective diffusivity and the colourimetric pH's response speed [30]. Higher swelling ratios can quicken the colourimetric response, but a swelling ratio that is too high may also cause the roselle extract to leach and compromise long-term signal stability [31]. Hence, the optimal swelling ratio needs to be studied to minimize the risk of leaching. Roselle extract anthocyanins do not exhibit toxicity to patients and are biocompatible [32]. While it is not toxic, the leaching may affect the smart bandage's ability to detect infections through pH over time. Hence, since anthocyanin leaching can be caused by swelling-induced water uptake and affect the reliability of the pH sensing, future development could consider peptide incorporation to strengthen the physical integrity of the hydrogel and also improve anthocyanin retention [33].

Anthocyanins typically have quinoid bases, flavylium cation, carbinol and pseudo bases. A rapid loss of quinoid bases occurs during increased pH values. Flavylium cations hydration also occurs as pseudo bases and carbinols are produced, which enters the colourless Chalcone balance [23]. This may contribute to the white colour observed at pH 7, where the colour intensity was lower than that observed at pH 6. The green colour observed at pH 6.5 and 7.5 also indicate that the colour response was influenced by factors beyond pH-dependent anthocyanin transformations. The similar colour intensity observed across pH 6.5–7.5 may be because the anthocyanin went through structural changes without producing a sufficiently distinct visual response within this pH range. However, the reappearance of pink at pH 8 does not follow the expected progressive colour transition of anthocyanins with increasing pH. This deviation may be attributed to a complex hydrogel environment, including interactions between anthocyanins and the hydrogel components, as well as possible non-uniform distribution of the extract within the matrix. Therefore, the observed hydrogel colour response cannot be directly correlated to pH based solely on the theoretical colour transitions of anthocyanins in solution.

Work by Nguyen et al. [13] produced anthocyanin-rich roselle extract that showed distinct colour change from pH 1 to 12. In that work, the extract showed a colour change from vivid red to orange red from pH 1 to 5 (acidic). When the solutions were at pH 6 to 7, the colour changed from orange red to reddish brown. When the solution was at pH 8 to 12, the solution changed from dark brown to greenish yellow. It was likely due to the different preparation methods. The main difference was that the extract was fermented by acetic acid bacteria and incubated. The bacterial cellulose that is synthesized by the acetic acid bacteria is biocompatible and biodegradable. Since it lacks lignin, hemicellulose and plant cell-wall components, it is suitable for food applications [34]. However, the suitability of integrating this extract into smart bandages is to be determined through future work. Optimizing the extract concentration, hydrogel composition and processing conditions can be done to improve the non-monotonic colour response.

The colours of the smart bandages were taken and matched with simulated dataset images, as shown in Figure 31.

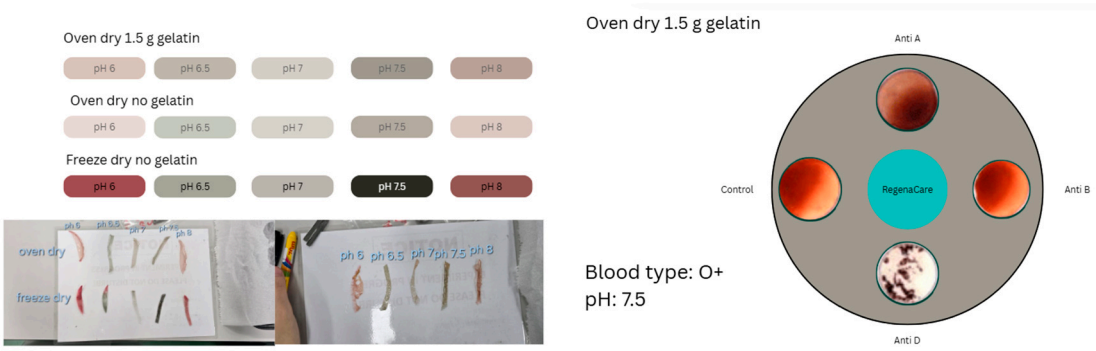

(**a**) (**b**)

Figure 31. pH simulated dataset. (**a**) Colour matching. (**b**) Simulated dataset for app sample.

Based on the simulated dataset, the RGB values are as shown in Table 7:

Table 7. RGB values of the smart bandage hydrogel at each pH, from the simulated dataset.

Drying Method	pH	R	G	B
Freeze-dry	6.0	147	78	81
Freeze-dry	6.5	164	164	152
Freeze-dry	7.0	184	179	173
Freeze-dry	7.5	47	47	39
Freeze-dry	8.0	137	88	84
Oven-dry (gelatin)	6.0	211	194	186
Oven-dry (gelatin)	6.5	186	182	171
Oven-dry (gelatin)	7.0	210	207	200
Oven-dry (gelatin)	7.5	156	154	142
Oven-dry (gelatin)	8.0	179	161	151
Oven-dry (no gelatin)	6.0	185	184	175
Oven-dry (no gelatin)	6.5	202	198	188
Oven-dry (no gelatin)	7.0	196	195	185
Oven-dry (no gelatin)	7.5	212	208	195
Oven-dry (no gelatin)	8.0	215	200	193

Since the colour response was non-monotonic across the tested pH range (pH 6–8), a calibration curve would not be meaningful at this stage since it requires a consistent monotonic relationship. Hence, improving the formulation of the roselle extract should be prioritized before constructing a calibration curve.

3.4.3. UV-Vis Data

Since most of the UV-Vis data remained constant at around 3.3 A, this suggested that the colour spectrum was above the machine's upper limit. Hence, a machine with a higher upper limit should be used in future experiments for further study to ensure accuracy. In the UV-Vis data, no monotonic relationship was observed between the pH and the onset wavelength of the absorbance decline, suggesting that this feature alone cannot distinguish between pH conditions in the current dataset. This confirms the visual observation by both pH and the smart bandage's colour changes that no clear pattern could be observed and confirms that the colour change is non-monotonic. In a separate study by Benvenuto et al. [35] which focused on anthocyanin-loaded PVA-films, the results demonstrated a strong near UV-absorption at approximately 270–380 nm. However, another weak broad band was also observed at the 520–550 nm range [35]. When the sugar molecules are removed from the anthocyanin, the structure that remains is called anthocyanidin, which is an aglycon structure. In another study by Gómez et al. [36], the results showed that from

200 to 700 nm, there were two peaks. One peak is in the visible region at 512 nm, and the second is in the lower-intensity absorbance band at approximately 251 nm. According to Gómez et al. [36], anthocyanidins generally have two main absorption bands, which are at 270–280 nm (band II) and 465–560 nm (band I), both in alcoholic solution and in the presence of hydrochloric acid. There is also a third band which peaks at 310–360 nm with a smaller intensity [36]. The peaks at 270–280 nm and 310–360 nm were consistent with literature results, but due to experimental limitations, the bands above 400 nm could not be observed. According to Li et al., anthocyanins have two main peaks at approximately 275 nm (UV region) and 500–540 nm (visible region) [37]. Since the results got cut off at 400 nm, the characteristics of anthocyanin's colour change in UV-Vis could not be fully studied. Hence, future work should expand the range of the UV-Vis when studying the characteristics of anthocyanins.

3.5. Failure Analysis and Limitations

3.5.1. Fabrication and Mechanical/Fluid Performance

During early membrane fabrication, an excessive initial gelatin concentration produced visible perforations in the hydrogel, compromising membrane integrity; this was mitigated by reducing the gelatin content, but indicates that the fabrication process is sensitive to formulation ratios and would benefit from tighter process control at scale. Tensile testing was performed on a single specimen per formulation rather than replicate specimens, due to sample and equipment availability constraints; as a result, the differences in tensile strength observed between formulations (Section 2) could not be statistically evaluated, and future work should include replicate testing to establish variability and confidence in these mechanical properties. Similarly, the preliminary swelling-behaviour screening used to select the final formulation was conducted as single runs rather than replicates and should be treated as indicative rather than statistically validated. Additional mechanical and fluid-handling properties relevant to wound-dressing performance, including tear resistance, flexibility under repeated flexion, adhesion to skin, barrier integrity against liquid ingress, and behaviour under repeated wear or removal were not evaluated, and independent fabrication batches were not compared to assess batch-to-batch consistency. The repeated value is near 3.3. A flat value at exactly 3.30 may indicate detector saturation or the instrument's upper reporting limit. Hence, a UV-Vis machine with a higher upper detection range may be used to further accuracy.

To protect the integrated electronics from liquid ingress and short-circuiting, a hydrophobic PVC layer was implemented in this prototype using a heat gun. PVC was chosen as a hydrophobic layer as the water-contact angle for untreated PVC is 82 ± 2° [38], while smoother or treated PVC can have a water-contact angle ranging from 103 to 157 ± 1.8°, suggesting it is moderately to strongly hydrophobic [39,40]. However, its performance as a long-term wearable biomedical interface warrants critical evaluation. According to Krongauz et al. [41], PVC films are used in medical and food packaging alongside other applications that need moisture and gas barriers. Their findings obtained diffusion coefficients ranging from 2.10×10^{-7} cm^2 s^{-1} in PVC with a glass transition temperature T_g = 274.2 K at 303 K, to 21.0×10^{-7} cm^2 s^{-1} in PVC with T_g = 266.0 K at 343 K. PVC does not have very high water diffusion, and even PVC that is free of plasticizers have a water sorption that is only slightly lower than those with plasticizers [41]. Kim et al. studied TPU/PVC gel on electronic sensors, and their findings indicated that at high temperatures, PVC gel is susceptible to plasticizer volatilization which can affect its stability in the long run [42]. According to Minale et al. [43], PVC can have a mass-loss step at temperatures near 270 °C due to dehydrochlorination and the formation of conjugated polyene sequences. A secondary degradation can even occur at higher temperatures as the PVC backbone

breaks down and can form chars [43]. To avoid destroying the electronic components by heating, the electronics were not embedded into the PVC layer but instead placed on top of it. Hence, while the heat gun may have been an option for proof-of-concept to produce a water barrier to prevent getting the electronics wet, better methods may be explored for future development. Studies by Kim et al. [42] and Minale et al. [43] blended TPU with PVC, but this could not be done due to lack of relevant equipment required for this process. However, it may be considered as an alternative in the future, besides considering replacing the PVC with better suited materials. According to Bakar et al., the market has shifted to polymeric substrates for screen-printed electrodes such as PVC as they provide mechanical flexibility allowing for the integration into wearables such as gloves and textile-based electrodes, making it more user friendly [44]. However, regarding compatibility with hydrogel, studies have experimentally demonstrated that PVC with hydrogel electrodes can make devices that are flexible but show mechanical deformation due to interfacial delamination between hydrogel electrodes and the PVC [42,45]. Although using a heat gun to heat the PVC is not conventional, it is similar to the concept of thermal welding. According to Mishuk et al. [46], PVC has a glass transition of approximately 90 °C, which was the approximate temperature of the heat gun setting. Since PVC has a temperature-dependent adhesion, the 90 °C allows the PVC to stick onto the hydrogel surface [46]. While the adhesion cannot be quantified due to experimental limitations, studies have shown that PVC has a certain temperature-dependent adhesion. Interfacial compatibility between the PVC layer and the hydrogel matrix was not investigated, as it was unnecessary for the scope of this study; the PVC functions strictly as a mechanical, waterproof barrier rather than a chemically integrated phase. In summary, PVC is flexible and can form a moisture barrier. However, due to its adhesion, compatibility with hydrogel and likelihood of degradation due to high temperature, it may be better to consider other materials or alternatives to form a thin, flexible and biocompatible waterproof layer.

3.5.2. System-Level Performance

The electronic subsystem was demonstrated to be powered via NFC energy harvesting with capacitor stabilisation, but key system-performance parameters were not characterised, including harvested power output, capacitor charging time, minimum operating voltage, effective NFC read range, data-transfer success rate, transmission latency, sensor sampling frequency, continuous operating duration, and compatibility across different smartphone models and NFC chipsets.

3.5.3. Sensor and Diagnostic Validation

Heart-rate and oxygen-saturation readings from the MAX30100 sensor were not validated against a reference pulse oximeter or ECG under controlled or clinically relevant conditions, so the accuracy of the physiological monitoring subsystem remains unconfirmed. For the colourimetric pH indicator, testing used qualitative visual observation rather than objective colour coordinates or absorbance values, was not conducted under controlled lighting, and used a limited number of samples per condition. Critically, the hydrogel's colour response across the clinically relevant pH 6–8 range was found to be non-monotonic. The colour intensity did not change consistently with increasing pH, which currently prevents the defining of a reliable diagnostic colour-to-pH threshold. The indicator has also not been tested in physiologically-relevant fluids such as saline, blood, wound exudate, or protein-containing solutions, which are known to affect anthocyanin behaviour.

3.5.4. Blood-Typing Subsystem

The image-processing algorithm for blood-type classification was developed and prototyped using synthetic, computer-generated card images rather than real blood samples; these synthetic images do not reproduce the visual texture, lighting variability, or agglutination patterns of real blood-typing reactions, so no accuracy figures are reported for this subsystem. Blood typing is currently performed externally through smartphone image analysis rather than an embedded sensor, which reduces hardware cost but introduces dependence on ambient lighting conditions and camera quality, a known limitation of smartphone-based colourimetric diagnostics [7].

3.5.5. Biological Safety

No cytotoxicity, antimicrobial, skin-contact safety, or sterility testing was performed on the hydrogel membrane, and no wound-healing model was used; claims regarding biocompatibility and antimicrobial function in this paper are therefore based on the known properties of the constituent materials reported in the literature rather than on data generated in this study (refer to Sections 1 and 3.3).

3.5.6. Reproducibility

Several fabrication and testing parameters that would be needed to independently reproduce this work were not systematically recorded or reported, including membrane thickness and casting area, roselle extract concentration/yield from the extraction process, the composition of the pH buffer solutions used in Section 4.5.4, and the image-acquisition conditions (lighting, camera, distance) used for colourimetric and blood-typing photography.

The long-term durability and wear-testing of the membrane and electronics beyond initial laboratory-scale mechanical and swelling tests have not yet been conducted, and the device has not undergone clinical or in vivo testing, both of which are necessary before regulatory approval [47,48] and clinical deployment can be pursued.

3.6. Electronics

The power output of 3.33 V is sufficient to operate the STM32F103C8T6 microcontroller chip (operating voltage: 2.0 to 6.0 V) with the MAX30100 sensor (operating voltage: 1.8 V to 3.3 V). While the communication of data from the NFC tag to the phone is extremely consistent with no issues, the accuracy and reading ranges need to be enhanced to make a more reliable system.

3.7. Future Perspective

The future development of RegenaCare should focus on replacing manually soldered copper connections with flexible printed circuits to reduce device bulk and rigidity, improving wearer comfort during prolonged use [49]. Expanding the training dataset used for the AI-based colourimetric and blood-typing analysis with a wider range of clinical wound images and lighting conditions could improve the robustness of the mobile application's image-processing pipeline, subject to validation across controlled lighting, camera types, and clinically representative images [7,50]. Additional physiological-sensing modalities, such as temperature and moisture sensors, alongside a dedicated colourimetric sensor using UV-Vis wavelength data, would further improve the accuracy and clinical utility of infection detection beyond the current roselle-based visual indicator. Finally, integrating cloud-based data storage and doctor–patient teleconsultation features into the mobile application would allow healthcare professionals to remotely monitor wound status and intervene earlier, extending RegenaCare from a standalone sensing device into a complete telehealth platform [50].

Additionally, to improve the observedcolourur change of the roselle hibiscus extract, further studies should investigate its anthocyanin concentration, as well as the effects of extract concentration, required extraction conditions, optimal storage conditions, light exposure and temperature. The roselle extract can be optimized by changing the preparation process, optimizing the extract concentration, hydrogel composition and processing conditions. As mentioned in Section 3.4.2, the incorporation of peptides may also be considered to improve the retention of roselle extract pigments, reducing the risk of leaching into wounds [33]. Another area for future work could involve comparing the performance of conventional electrode-based pH sensors with that of roselle extract to evaluate their respective suitability for integration into a low-cost, battery-free smart bandage. In addition to that, the hydrogel can be optimized further to improve the PVA to gelatin ratio, hydrogel swelling, thickness, anthocyanin loading and diffusion behaviour as well as matrix composition. Co-pigmentation using compounds such as p-coumaric, cinnamic and ferulic acids may improve anthocyanin colour stability and intensity [23]. NFC energy harvesting can also be enhanced to improve the reading range and accuracy of the MAX30100 sensor. Future work may also focus on optimizing the optical characterization parameters of the anthocyanin-based colourimetric system. To comprehensively map the quantitative relationship between pH variations and visible color shifts, subsequent studies will utilize an expanded wavelength tracking range of 400–700 nm to fully capture the characteristic visible absorption bands. Furthermore, systematic sample dilution strategies and adjusted optical path lengths will be deployed to ensure all spectral data remain well within the linear dynamic range of the detector, completely mitigating the risk of saturation at peak maximum.

Addressing the limitations identified in Section 3.5 should be prioritized in the following order: replicate mechanical and swelling testing ($n \geq 3$, independent fabrication batches) to establish statistical confidence in formulation comparisons; the characterization of NFC system performance (range, power, latency, data-transfer reliability) on the bench; validation of the MAX30100 heart-rate/SpO2 readings against a reference device; objective, lighting-controlled colourimetric calibration of the pH indicator in physiologically relevant fluids, specifically targeting the non-monotonic pH 6–8 response before any diagnostic threshold is proposed; blinded validation of the blood-typing algorithm against real, known blood-group samples, rather than synthetic training images; cytotoxicity and antimicrobial testing against defined microorganisms with appropriate controls, as a prerequisite for any future biocompatibility or antimicrobial claims. The waterproof layer may also be further developed as PVC may not be the best choice due to its likelihood of degrading at high temperatures and adhesion.

Additionally, testing can be done as a future development to assess the smart bandage's ability to remain functional despite repeated movement, hydration, mechanical deformation and prolonged skin contact. This can be done by assessing the adhesion of the wound contact layer after a prolonged amount of time on a wearer and repeating the hydrogel swelling test in fluids that simulate body fluids such as blood and sweat. While testing was done in water to test the hydrogel under simple conditions during prototyping, future development may test the hydrogel in compositions more similar to wound exudate, which can be simulated with salts, proteins, enzymes, and other biological components. This is essential as switching from water to wound exudate environment may provide information on its influence on the hydrogel's behaviour. The SEM imaging of different hydrogel cross-sections and quantitative pore-size analysis may also further explain the processing conditions, microstructure, swelling, and mechanical properties.

4. Materials and Methods

4.1. Materials and Design Selection

The materials used to fabricate the RegenaCare hydrogel membrane, and their primary functions are summarized in Table 8, while the equipment used are stated in Table 9.

Table 8. Materials used and their primary functions.

Material	Function
Polyvinyl Alcohol (PVA) (PVA; average molecular weight = 89,000–98,000 g/mol, 99+% hydrolyzed, density 1.19–1.31 g/cm^3, CAS 9002-89-5) was purchased from Sigma-Aldrich (St. Louis, MO, USA).	Forms the main hydrogel matrix and provides mechanical strength, flexibility and moisture retention.
Glycerine (glycerol; purity ≥99.5%, molecular weight 92.09 g/mol, density 1.25 g/mL, CAS 56-81-5) was obtained from Merck KGaA (Darmstadt, Germany)	Increase flexibility and elasticity of hydrogel, prevents brittleness and cracking.
Aloe Vera	Promotes healing, antibacterial and anti-inflammatory properties, also accelerates tissue regeneration.
Gelatin (Gelatin; 8 - 13% moisture, density 1.3–1.4 g/cm^3, CAS NO 9000–70–8 was purchased from take it global, Malaysia)	Improves biocompatibility with human skin, also supports tissue regeneration and increases hydrogel's water adsorption ability.
PVC plastic wrap (was purchased from NISO, Malaysia)	Acts as a hydrophobic barrier to improve mechanical stability and moisture resistance, ensuring that no water penetrates the embedded electronic components.
Dried Hibiscus Roselle Flowers	Acts as a pH indicator as it provides natural pH responsive anthocyanin pigments, enabling visual monitoring of wound status or presence of infection. Extract also provides antioxidant and antimicrobial properties that support wound healing.
Heart-Rate Sensor (MAX30100 Oximeter) (IC manufactured by Analog Devices, Wilmington, MA, USA; module procured from Robotronik, Kuala Lumpur, Malaysia)	Measures heart rate and blood flow to indicate patients' blood circulation or presence of infection during wound healing. 1. Beats per minute (BPM): Measures how fast your heart bumps in a single 60 s window 2. Perfusion Index (PI): Indicates the strength of blood flow to the tissue 3. Accelerated Photoplethysmography (APPG): Detects subtle vascular changes
Microcontroller (STM32F103C8T6) (Type C port design, 25.40 mm × 22.86 mm microcontroller IC by STMicroelectronics, Geneva, Switzerland; breakout board manufactured by DIYMore, Shenzhen, China)	Collects data from sensors and processes the signals.
NFC Sensor (ST25DV16K) (NFC IC by STMicroelectronics, Geneva, Switzerland; breakout board manufactured by DIYMore, Shenzhen, China)	Enables wireless communication between the smart bandage and smartphone. It receives processed data from the microcontroller and sends them to a custom mobile app where the patient's health and wound condition and information is stored, displayed and monitored without removing the bandage.
Blood Type Card (c4k_store, Indonesia)	A disposable card containing four reagent circles, Anti-A, Anti-B, Anti-D and control, which are used to identify a patient's ABO and Rh blood type. The card image is captured through the app where the Python 3.11.9 image-processing algorithm will analyze the agglutination pattern to determine and display the blood type. This allows the healthcare system to be able to access critical patient information quickly during emergency treatment. Note: Only General-Trauma wound membrane has the blood type features

Table 9. List of equipment used.

Equipment	Function	Category
Stuart SWB15D Digital Water Bath (Stuart Equipment, Stone, Staffordshire, UK)	Provides controlled heating conditions during hydrogel preparation.	Membrane fabrication
Scanvac CoolSafe Freeze Dryer by LaboGene (ScanVac CoolSafe, LaboGene ApS, Allerød, Denmark)	Removes water from the hydrogel through sublimation to produce a dried porous structure.	Membrane fabrication
Elmasonic P multifrequency Ultrasonication Machine (Elma Schmidbauer GmbH, Singen, Germany)	Uses ultrasonic waves to improve mixing and dispersion of materials and also remove the air bubbles in the hydrogel mixture by degassing.	Membrane fabrication
IKA RW 20 Digital Mechanical Overhead Stirrer (IKA-Werke GmbH & Co. KG, Staufen, Germany)	Ensure proper mixing of PVA when heated in water bath.	Membrane fabrication
Heidolph Hei-PLATE Mix 'n' Heat Core+Magnetic Hotplate Stirrer (Heidolph Instruments GmbH & Co. KG, Schwabach, Germany)	Ensure homogenous mixing of materials such as PVA, gelatin, roselle hibiscus extract, glycerol and aloe vera.	Membrane fabrication
Memmert UN75 Universal Laboratory Oven (Memmert GmbH + Co. KG, Schwabach, Germany)	Oven-drying process	Membrane fabrication
Freezer	Freeze–thawing process	Membrane fabrication
INSTRON 5969 Dual Column Universal Testing Machine (UTM) (Instron Corporation, Norwood, MA, USA)	Evaluates the mechanical properties of the hydrogel including tensile strength, elongation and flexibility to ensure that the smart bandage can withstand high stress.	Testing
Weighing scale (Mettler-Toledo GmbH, Greifensee, Switzerland & BEL Engineering s.r.l., Monza, Italy)	Used for hydrogel swelling test and weighing materials during membrane fabrication.	Membrane testing and membrane fabrication

4.2. Hydrogel Membrane Fabrication

4.2.1. Roselle Extraction

A total of 25 g of dried roselle hibiscus flowers are grinded until a powder forms. The powdered roselle hibiscus is poured into 120 mL of ultra-pure water and placed into a water bath at 60 °C for 30 min. The solution is then filtered out using filter paper and collected.

4.2.2. Hydrogel Membrane Fabrication

The hydrogel membrane was fabricated using 150 mL of ultra-pure water, 6.67 g of PVA, 5 mL of glycerine, 4 g of aloe vera, 1.5 g of gelatin and 22 mL of roselle hibiscus extract. PVA was first dissolved in ultra-pure water at 90 °C using a water bath and mechanical stirrer at 200 to 250 rpm. The gelatin was then added and put into the water bath at 60 °C until dissolved, before adding the aloe vera, roselle hibiscus extract and glycerine. The mixture was ultrasonicated to disperse the components and remove air bubbles, first at a degas setting for 1 h and a sweep setting for 30 min, poured into Petri dishes, and subjected to either a freeze–thawing or oven-drying method. The fabrication of the hydrogel membrane was inspired by the Janus structure where there are two distinct opposing faces or layers on a single material with one side being hydrophilic (water-attracting) and the other hydrophobic (water-repelling).

4.2.3. Freeze–Thawing and Freeze-Drying

The freeze–thaw cycle was conducted at −20 °C for three cycles, as shown in Table 10:

Table 10. Freeze–thaw cycle durations.

Cycle	Freeze	Thaw
1	4 h	1 h
2	15 h	1 h Note: sped up by putting in a tray over a water bath of approximately 60 °C (no lid)
3	4 h	1 h

The freezing–thaw cycle took a total of 26 h. After the freeze–thaw cycles, the Petri dishes had to be pre-freezed at −80 °C for at least 24 h before being placed in the freeze dryer at −100 °C for 24 h. The freeze–thaw cycle was initially conducted at −20 °C rather than immediately at −80 °C to allow gradual ice-crystal nucleation and growth throughout the hydrogel. As the water freezes, the ice crystals act as temporary method [44] templates, and the polymer chains are concentrated around them. After the ice is removed during freeze-drying, an interconnected, sponge-like porous texture is formed. This porous structure improves the membrane's ability to absorb and retain wound exudate. Freezing directly at −80 °C may cause rapid solidification and the formation of smaller, less uniformly distributed ice crystals, which can produce a denser or less interconnected pore structure and may increase thermal stress within the membrane. Following the freeze–thaw cycles, the membranes were pre-frozen at −80 °C for at least 24 h to ensure that all remaining water was completely solidified before freeze-drying. This step was important because freeze-drying requires the frozen water to undergo sublimation directly from ice to vapour. Complete pre-freezing helps preserve the ice-templated porous structure, prevents partial melting or structural collapse during drying, and produces a more uniform and stable membrane.

4.2.4. Oven-Drying

An alternative method of drying the membrane was the oven-drying (60 °C) method. The hydrogels were put into an oven at 60 °C for 48 h.

4.2.5. Hydrophobic Layer

PVC was chosen as a hydrophobic layer as the water-contact angle for untreated PVC is 82 ± 2° [38], while smoother or treated PVC can have a water-contact angle ranging from 103 to 157 ± 1.8°, suggesting it is moderately to strongly hydrophobic [39,40]. The procedure for applying the PVC book wrap on the hydrogel membrane using a heat gun was performed by uniformly applying heat until a waterproof barrier is created to protect the wound site from external contaminants.

The hydrogel membrane surface is cleaned to remove dust and moisture. The PVC is cut according to the circumference hydrogel membrane. The PVC is positioned evenly over the hydrogel membrane. The heat gun is then set to a low temperature setting (approximately 90 °C) and held approximately 10–20 cm above the hydrogel membrane as high temperature can soften or deform both PVC film and hydrogel membrane. This is to reduce the risks of melting PVC and damaging the hydrogel membrane. The heat gun is moved continuously around to ensure the heat is distributed evenly. This process must be done quickly as prolonged heating exposure may lead to the excessive shrinkage, warping or degradation of gelatin. This process is continued until the PVC fully conforms to the hydrogel membrane

surface. The hydrogel membrane is then left to cool. For the freeze-dried membrane, the PVC layer was sewn on instead to avoid damaging the freeze-dried hydrogel.

4.3. Electronic Subsystem Design and Assembly

The electronic subsystem, as shown in Figure 32, consists of an STM32F103C8T6 microcontroller (Type C port design, 25.40 mm × 22.86 mm microcontroller IC by STMicroelectronics, Geneva, Switzerland; breakout board manufactured by DIYMore, Shenzhen, China), a MAX30100 heart-rate (IC manufactured by Analog Devices, Wilmington, MA, USA; module procured from Robotronik, Kuala Lumpur, Malaysia) and oxygen-saturation sensor, and an ST25DV16K NFC tag (NFC IC by STMicroelectronics, Geneva, Switzerland; breakout board manufactured by DIYMore, Shenzhen, China).. NFC was selected over Bluetooth and Wi-Fi because it simultaneously enables wireless communication and energy harvesting, allowing the system to operate without an external battery. For the general-trauma wound variant, blood typing is performed externally using a smartphone camera and a disposable blood-typing card (Anti-A, Anti-B, Anti-D and control reagent circles) rather than an embedded blood sensor, reducing hardware complexity and cost; this feature is omitted from the diabetic-ulcer variant. The bandage adopts a two-layer structure: an inner hydrophilic hydrogel layer in contact with the wound for exudate absorption and a preliminary qualitative colour indication related to pH, and an outer hydrophobic layer housing the electronic components and protecting them from moisture.

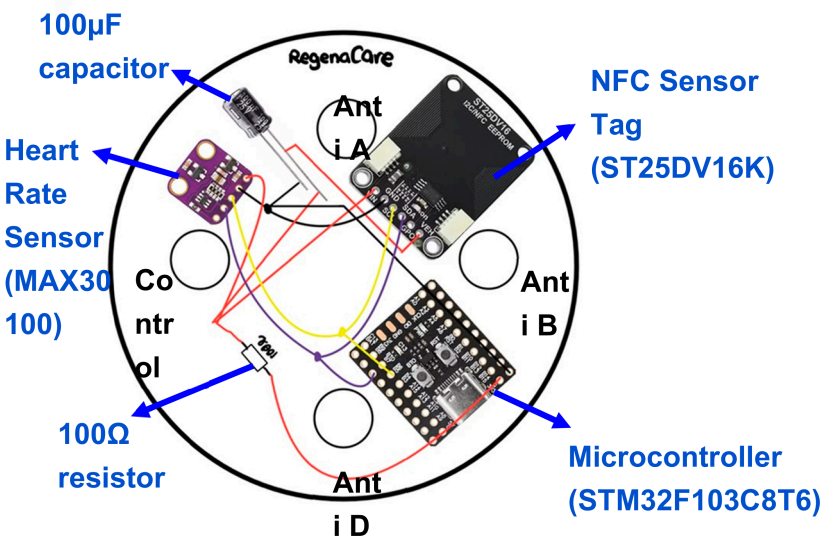

Figure 32. Circuit diagram

The MAX30100 sensor was chosen mainly because its power requirement fit the NFC energy harvesting's power output; it did not need to be clipped on, allowing user convenience; and to ensure it is compact. The MAX30100 is designed for photoplethysmographic measurements, whose performance depends strongly on optical coupling, tissue contact, and measurement geometry. It is positioned on top of the PVC layer of the smart bandage, but a small hole was cut through the wound contact layer to ensure the sensor's red light can be used for photoplethysmographic measurements. Due to this, it is essential to ensure that the hydrophobic layer is completely transparent to ensure it does not obstruct the pH colourimetric response or the MAX30100's photoplethysmographic measurements. The MAX30100 sensor measures beats per minute (BPM), perfusion index (PI) and accelerated photoplethysmography (APPG). These measurements allow the doctors to know the wound's circulatory status and tissue perfusion, and ensure adequate blood flow and

oxygen delivery are for wound healing, thereby reducing the risk of postoperative infections. This is because sufficient oxygenation of the wound can aid the healing process [9]. The MAX30100 sensor readings were compared with a smartwatch's BPM for calibration, but future development is required to further calibrate it, as while the sensor can detect readings accurately, it is not consistent. The layers of the smart bandage and its exploded view are shown in Figures 33 and 34.

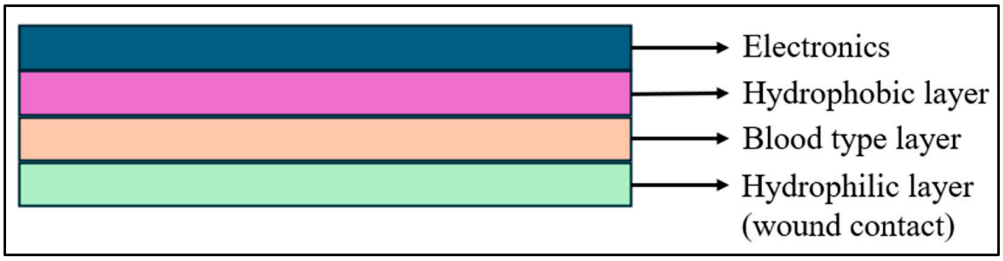

Figure 33. Detail drawing of layers of the bandage.

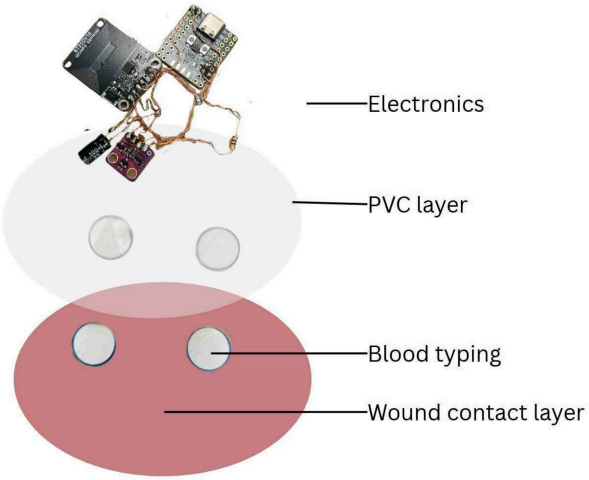

Figure 34. Exploded view of bandage layers.

The exploded view shows the arrangement of the layers. The electronics that were soldered together with copper wire were placed onto the PVC layer, with the blood-typing layer placed between the wound contact layers.

The phone used for testing was an Android Samsung Galaxy S24 Ultra. Multiple videos were taken while measuring the power output with a multimeter to record the range of energy harvested and the capacitor charging time. To avoid short-circuiting the electronics, the wires were covered with a layer of transparent nail polish to provide a layer of insulation.

4.4. Mobile Application

The companion mobile application was developed using HTML, CSS and JavaScript for the front-end dashboard, which displays patient information, sensor readings and wound-monitoring data, while the STM32F103C8T6 microcontroller (Type C port design, 25.40 mm × 22.86 mm microcontroller IC by STMicroelectronics, Geneva, Switzerland; breakout board manufactured by DIYMore, Shenzhen, China)was programmed in C to control the sensors and communicate with the application. Backend processing, including pH detection and blood-type analysis, was implemented in Python 3.11.9 using the OpenCV library. Wound pH is estimated from the median RGB values in a defined region in the mem-

brane image adjacent to the blood-type circles, avoiding interference from agglutination or other artefacts. The workflow of the app is as shown in Figure 35.

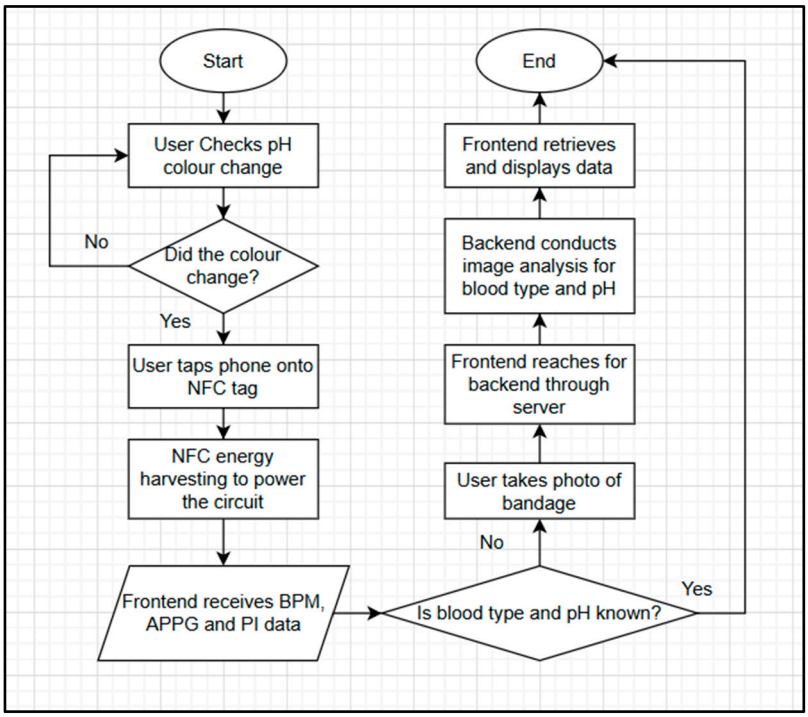

Figure 35. App workflow.

4.5. Property Testing

4.5.1. Swelling Test

The sample weight was recorded before soaking each membrane in water, and weight was subsequently measured every hour over a five-hour period to determine the swelling ratio, defined as the ratio of hydrated weight to initial dry weight, for both oven-dried and freeze-dried samples with and without gelatin.

The original mass of the hydrogel is weighed and recorded. The hydrogel is placed in water and weighed every 1 h for 5 h. For the final roselle-incorporated formulation, three independent specimens were tested per formulation ($n = 3$); results are reported as mean ± standard deviation. Preliminary formulation-screening trials without roselle extract (Section 3.1, Table 2) were conducted as single runs and are reported as individual values only. The experiment was conducted at room temperature (approximately 25 °C). Data for humidity levels in the room were not available.

4.5.2. Tensile Testing

Mechanical performance was evaluated using a Universal Testing Machine (UTM) on freeze-dried and oven-dried membranes, with and without 1.5 g gelatin reinforcement, to obtain stress–strain curves, tensile strength, and elongation at break.

The hydrogel membranes are cut into rectangular strips using a sharp blade or cutter. The samples are prepared with approximate dimensions of 40–50 mm length and 5–10 mm width. The membrane thickness is measured at three different points using a digital caliper and the average thickness is recorded. The samples are lightly hydrated with distilled water by dipping it briefly before testing to simulate wound conditions and reduce brittle fracture during testing. Small reinforcing end tabs with 1 to 1.5 cm length and 1.5 cm width are prepared using cardstock and masking tape. The reinforcing tabs are attached to both

ends of the hydrogel sample to improve grip and prevent slippage during testing. The reinforcing tabs at both ends are placed between the upper and lower screw-type grips of the INSTRON 5969 Dual Column Universal Testing Machine (UTM) manufactured in the United States. The grips are tightened gradually and evenly to secure the sample without causing pre-damage to the hydrogel. The sample is aligned vertically to ensure a uniform load distribution during testing. Tensile testing is conducted at room temperature using a Universal Testing Machine. The crosshead speed is set to 5 mm/min. The sample is stretched continuously until complete failure or breakage occurs. Force and displacement data are recorded throughout the experiment. Their tensile strength, elongation at break, and Young's modulus are calculated from the stress–strain curve. One specimen was tested per formulation due to sample and equipment availability constraints.

4.5.3. Fourier-Transform Infrared Spectroscopy (FTIR)

FTIR spectra were recorded over the range 4000–650 cm^{-1} for gelatin-only, aloe vera-only, and combined aloe vera + gelatin samples (with and without roselle extract, oven- and freeze-dried, and a non-homogeneously stirred defective sample) to characterize the major functional-group bands, compare formulations of the membranes and identify the effect of formulation and drying method on functional groups. The FTIR machine used was PerkinElmer Spectrum IR Version 10.7.2, which was manufactured in the United States.

4.5.4. pH Indicator Testing

All the experiments were conducted at room temperature (approximately 25 °C).

Roselle Hibiscus Extract Colour Change

A few pH buffer solutions (pH 1, 6, 6.5, 7.5, 8 and 11) are prepared and labeled. A few drops of roselle extract are dropped into a different pH solution. Any colour changes are observed and recorded.

Smart Bandage Colour Change

A few pH buffer solutions (pH 6, 6.5, 7, 7.5 and 8) are prepared and labeled. The hydrogel patches are cut into equal-sized samples. The initialcolourur of each patch are recorded. Each patch is placed into a different pH solution. The samples are allowed to react for a fixed time (approximately 1 to 2 min). Any color changes are observed and recorded. The patches are using forceps. The samples are photographed and results documented.

5. Conclusions

This work presents RegenaCare as a proof-of-concept prototype integrating a PVA–gelatin–aloe vera–roselle hydrogel membrane with an NFC-enabled electronic subsystem and a companion mobile application for future wound-monitoring applications. The fabricated membranes achieved tensile strengths of 4.91–6.34 MPa, exceeding the 0.5–1.5 MPa design target. Freeze-dried formulations generally showed greater swelling than oven-dried formulations, with the final roselle-incorporated, gelatin-free freeze-dried formulation reaching 6.23 ± 0.74 (mean ± SD, $n = 3$) at equilibrium, compared to 4.12 ± 0.82 for the equivalent oven-dried formulation. The oven-dried, gelatin-reinforced formulation showed the highest tensile strength recorded (6.3–6.34 MPa, single specimen). This indicated that formulation and drying methods could be tailored to different use requirements, but wound-type-specific suitability remains to be tested. The FTIR spectra supported gelatin incorporation through the appearance of amide-associated bands; attribution of roselle-specific features remains tentative because several formulation components have overlapping absorptions. The integrated prototype containing the STM32F103C8T6 micro-

controller, MAX30100 sensor, and ST25DV16K NFC module were configured to support NFC-powered wireless transmission of sensor data. The main strengths of this work are its low cost, its battery-free NFC design, and the combination of a mechanically characterised hydrogel, a colourimetric indicator, physiological sensing and a smartphone workflow in one platform. The gelatin-containing membranes also showed high extensibility, which is relevant to a dressing that must move with the skin. However, transmission reliability and wound-status classification were not validated. The main weaknesses of this work were the non-monotonic colour response, lack of calibration curve of RGB data, UV-Vis limitations, and lack of biocompatibility, antimicrobial or clinical testing. The estimated manufacturing cost was approximately RM51.50 per unit. These results demonstrate the technical feasibility of fabricating and integrating an affordable prototype bandage platform; they do not yet establish its diagnostic accuracy, clinical suitability, or long-term performance. Future work should first optimize the extract concentration, hydrogel composition and processing conditions to obtain a reliable colour–pH relationship, followed by calibration under controlled lighting in wound-relevant fluids. In parallel, replicate mechanical testing, the characterization of the NFC subsystem, validation of the sensors against reference devices, and cytotoxicity and antimicrobial testing are needed. If these are met, the platform could be applied to remote monitoring of chronic wounds such as diabetic foot ulcers and, through its blood-typing feature, to emergency trauma care. These results demonstrate the technical feasibility of fabricating and integrating an affordable prototype bandage platform; they do not yet establish diagnostic accuracy, clinical suitability, or long-term performance. Addressing the limitations mentioned in Section 3.5, particularly clinical validation and durability testing, represents the key next step toward real-world deployment for general-trauma wounds (such as car accidents), post-operative monitoring and diabetic ulcers.

Author Contributions: Conceptualization, J.H.T., J.A., P.T.W., M.U.Q. and M.M.; methodology, J.H.T., P.T.W. and M.M.; software, J.H.T.; validation, M.U.Q.; formal analysis, J.H.T. and M.M.; investigation, J.H.T., J.A., P.T.W., M.U.Q. and M.M.; resources, S.S.A.K.; data curation, M.U.Q.; writing—original draft preparation, J.H.T., P.T.W. and M.M.; writing—review and editing, J.H.T.; visualization, J.H.T.; supervision, S.S.A.K.; project administration, J.H.T.; funding acquisition, S.S.A.K. All authors have read and agreed to the published version of the manuscript.

Funding: This research received no external funding. However, the publication fee is funded by Taylor's University publication fund.

Institutional Review Board Statement: Not applicable.

Informed Consent Statement: Not applicable.

Data Availability Statement: The data presented in this study are available on request from the corresponding author.

Acknowledgments: The authors would like to thank Taylor's University for providing laboratory equipment and facilities, and Sachin Sharma Ashok Kumar for his supervision and guidance throughout this project. During the preparation of this manuscript/study, the authors used Claude AI, Sonnet 5 for the purposes of polishing language and Gemini AI, Auto AI for the purpose of improving image quality. The authors have reviewed and edited the output and take full responsibility for the contents of this publication.

Conflicts of Interest: The authors declare no conflicts of interest.

Abbreviations

The following abbreviations are used in this manuscript:

PVA	Polyvinyl Alcohol
FTIR	Fourier-transform infrared
NFC	Near-Field Communication
PVC	Polyvinyl Chloride
UV-Vis	Ultraviolet-Visible (Spectroscopy)
SD	Standard Deviation
ECG	Electrocardiogram
RM	Malaysian Ringgit

References

1. Gianino, E.; Miller, C.; Gilmore, J. Smart wound dressings for diabetic chronic wounds. *Bioengineering* **2018**, *5*, 51. [CrossRef] [PubMed]
2. Ministry of Health Malaysia. *National Health and Morbidity Survey (NHMS)*; Ministry of Health Malaysia: Shah Alam, Malaysia, 2020.
3. Mostafalu, P.; Tamayol, A.; Rahimi, R.; Ochoa, M.; Khalilpour, A.; Kiaee, G.; Yazdi, I.K.; Bagherifard, S.; Dokmeci, M.R.; Ziaie, B.; et al. Smart bandage for monitoring and treatment of chronic wounds. *Small* **2018**, *14*, 1703509. [CrossRef] [PubMed]
4. Sadeghi, A.; Molavi, A.M.; Nokhasteh, S.; Harati, Z. Advances in pH sensors for smart wound dressings. *Polym. Bull.* **2022**, *80*, 5831–5859. [CrossRef]
5. Wang, X. Colorimetric pH sensing materials for wound monitoring. *Biosens. Bioelectron.* **2019**, *126*, 433–441.
6. Rahimi, R.; Brener, U.; Ochoa, M.; Ziaie, B. Flexible and transparent pH monitoring system with NFC communication for wound monitoring. In Proceedings of the IEEE International Conference on Micro Electro Mechanical Systems (MEMS), Las Vegas, NV, USA, 22–26 January 2017.
7. Ehtesabi, H.; Kalji, S.-O.; Movsesian, L. Smartphone-based wound dressings: A mini-review. *Sensors* **2022**, *8*, e09876. [CrossRef] [PubMed]
8. Su, R.; Wang, L.; Han, F.; Bian, S.; Meng, F.; Qi, W.; Zhai, X.; Li, H.; Wu, J.; Pan, X.; et al. A highly stretchable smart dressing for wound infection monitoring and treatment. *Mater. Today Bio* **2024**, *26*, 101107. [CrossRef] [PubMed]
9. Sen, C.K. Wound healing essentials: Let there be oxygen. *Wound Repair Regen.* **2009**, *17*, 1–18. [CrossRef] [PubMed]
10. Berry, C.; Gallagher, J.M.; Goodloe, J.M.; Dorlac, W.C.; Dodd, J.; Fischer, P.E. Prehospital Hemorrhage Control and Treatment by Clinicians: A Joint Position statement. *Prehospital Emerg. Care* **2023**, *27*, 544–551. [CrossRef] [PubMed]
11. National Blood Authority Australia. *National Statement for the Emergency Use of Group O Red Blood Cells*; National Blood Authority Australia: Canberra, Australia, 2023.
12. Xu, G.; Lu, Y.; Cheng, C.; Li, X.; Xu, J.; Liu, Z.; Liu, J.; Liu, G.; Shi, Z.; Chen, Z.; et al. Battery-Free and wireless smart wound dressing for wound infection monitoring and electrically controlled On-Demand drug delivery. *Adv. Funct. Mater.* **2021**, *31*, 2100852. [CrossRef]
13. Nguyen, T.; Nguyen, D.; Tran, T.T.V.; Cao, A.; Luong-Nguyen, P.; Lam, N.D.; Ly, T.; Do, A.D.; Nguyen, Q. Fabrication of pH-Sensitive Bacterial Cellulose Films by Acetic Acid Fermentation of Anthocyanin-Rich Roselle (*Hibiscus sabdariffa* L.) Extracts for Real-Time Monitoring of Chicken Meat Spoilage. *J. Food Sci.* **2026**, *91*, e71030. [CrossRef] [PubMed]
14. Zheng, C.; Liu, C.; Chen, H.; Wang, N.; Liu, X.; Sun, G.; Qiao, W. Effective wound dressing based on Poly (vinyl alcohol)/Dextran-aldehyde composite hydrogel. *Int. J. Biol. Macromol.* **2019**, *132*, 1098–1105. [CrossRef] [PubMed]
15. Yang, T.B.; Tan, Z.; Chen, X.; Wang, F.B.; Tao, R.B.; Tong, Y.; Wang, X.; Fan, H.; Yu, M.; Zhu, Z. Skin Stretching Techniques: A review of Clinical application in Wound repair. *Plast. Reconstr. Surg. Glob. Open* **2024**, *12*, e6405. [CrossRef] [PubMed]
16. Kalra, A.; Lowe, A. Mechanical Behaviour of skin: A review. *J. Mater. Sci. Eng.* **2016**, *5*, 1000254. [CrossRef]
17. Capanema, N.S.V.; Mansur, A.A.P.; Carvalho, I.C.; Carvalho, S.M.; Mansur, H.S. Bioengineered Water-Responsive Carboxymethyl Cellulose/Poly(vinyl alcohol) Hydrogel Hybrids for Wound Dressing and Skin Tissue Engineering Applications. *Gels* **2023**, *9*, 166. [CrossRef] [PubMed]
18. Ratwani, C.R.; Donato, K.Z.; Grebenchuk, S.; Mija, A.; Novoselov, K.S.; Abdelkader, A.M. Enhanced Self-Healing in dual network entangled hydrogels by macromolecular architecture and alignment of surface functionalized HBN nanosheets. *Adv. Mater. Interfaces* **2024**, *12*, 202400691. [CrossRef]
19. Sancakli, A.; Basaran, B.; Arican, F.; Polat, O. Effects of bovine gelatin viscosity on gelatin-based edible film mechanical, physical and morphological properties. *SN Appl. Sci.* **2021**, *3*, 1–11. [CrossRef]
20. Masri, S.; Maarof, M.; Mohd, N.F.; Hiraoka, Y.; Tabata, Y.; Fauzi, M.B. Injectable crosslinked Genipin Hybrid Gelatin–PVA hydrogels for future use as BioINKs in expediting cutaneous Healing Capacity: Physicochemical Characterisation and Cytotoxicity evaluation. *Biomedicines* **2022**, *10*, 2651. [CrossRef] [PubMed]

21. Hanif, W.; Hardiansyah, A.; Randy, A.; Asri, L.A.T.W. Physically crosslinked PVA/graphene-based materials/aloe vera hydrogel with antibacterial activity. *RSC Adv.* **2021**, *11*, 29029–29041. [CrossRef] [PubMed]
22. Lema, A.A.; Mahmod, N.H.; Khandaker, M.M.; Abdulrahman, M.D. Roselle anthocyanin stability profile and its potential role in post-harvest deterioration: A review. *Plant Sci. Today* **2021**, *9*, 119–131. [CrossRef]
23. Kenawy, E.-R.S.; Kamoun, E.A.; Ghaly, Z.S.; Shokr, A.-B.M.; El-Meligy, M.A.; Mahmoud, Y.A.-G. Novel Physically Cross-Linked Curcumin-Loaded PVA/Aloe vera Hydrogel Membranes for Acceleration of Topical Wound Healing: In Vitro and In Vivo Experiments. *Arab. J. Sci. Eng.* **2022**, *48*, 497–514. [CrossRef]
24. Fallah, N.; Aarabi, A.; Dizaji, H.Z.; Ghashang, M. Development of a Colorimetric Intelligent Film Based on Biodegradable Polymers Incorporated with *Hibiscus sabdariffa* Anthocyanins for Monitoring Salmon Fish Spoilage. *Food Bioprocess Technol.* **2025**, *18*, 4632–4648. [CrossRef]
25. Lopes, P.M.; Mare, L.; Barbu-Tudoran, L.; Gadja, A.; Popescu, V. Gelatin hydrogel pH sensors incorporating anthocyanins for intelligent food packaging: Towards enhanced food spoilage detection. *Gels* **2026**, *12*, 292. [CrossRef] [PubMed]
26. Rosales-Murillo, S.; Sánchez-Bodón, J.; Olmos, S.H.; Ibarra-Vázquez, M.; Guerrero-Ramírez, L.; Pérez-Álvarez, L.; Vilas-Vilela, J. Anthocyanin-Loaded polymers as promising Nature-Based, responsive, and bioactive materials. *Polymers* **2024**, *16*, 163. [CrossRef] [PubMed]
27. Enaru, B.; Drețcanu, G.; Pop, T.D.; Stănilă, A.; Diaconeasa, Z. Anthocyanins: Factors affecting their stability and degradation. *Antioxidants* **2021**, *10*, 1967. [CrossRef] [PubMed]
28. Amperawati, S.; Hastuti, P.; Pranoto, Y.; Santoso, U. The Anthocyanins Content, Colour Changes and Thermal Stability of Roselle (*Hibiscus sabdariffa* L.) Petal Extract. *Int. J. Sci. Res. (IJSR)* **2019**, *8*, 428–435.
29. Wu, H.-Y.; Yang, K.-M.; Chiang, P.-Y. Roselle anthocyanins: Antioxidant properties and stability to heat and pH. *Molecules* **2018**, *23*, 1357. [CrossRef] [PubMed]
30. Sipahli, S.; Mohanlall, V.; Mellem, J.J. Stability and degradation kinetics of crude anthocyanin extracts from *H. sabdariffa*. *Food Sci. Technol.* **2017**, *37*, 209–215. [CrossRef]
31. Zhu, J.-L.; Yang, Y.; Mo, Y.; Chen, C.-H.; Hald, E.; Sheu, C.-L. Biobased Polymer Composites for Sensor-Integrated Wound Dressings: Structural roles, sensing interfaces and validation challenges. *Polymers* **2026**, *18*, 2607. [CrossRef]
32. Pisheh, H.R.; Rezaeian, R.; Sani, M.; Mohammadi, H. Smart colorimetric wound dressing for real-time infection detection and monitoring. *J. Biol. Eng.* **2026**, *20*, 1–20. [CrossRef] [PubMed]
33. Malar, D.S.; Prasanth, M.I.; Verma, K.; Prasansuklab, A.; Tencomnao, T. Hibiscus sabdariffa Extract Protects HaCaT Cells against Phenanthrene-Induced Toxicity through the Regulation of Constitutive Androstane Receptor/Pregnane X Receptor Pathway. *Nutrients* **2022**, *14*, 3829. [CrossRef] [PubMed]
34. Li, W.; Yang, Y.; Qi, Q.; Chen, X.; Huang, Y.; Chen, H.; Huang, J.; Chen, P. Improving the functional performance of anthocyanin indicator films through antimicrobial peptides incorporation: Enhanced stability, swelling control, and antibacterial efficacy. *Food Chem. X* **2025**, *32*, 103259. [CrossRef] [PubMed]
35. Benvenuto, M.; Desiderio, G.; Pane, A.; Cofone, F.; La Deda, M.; Gennari, O. Transparent Anthocyanin–PVA indicator films for Real-Time pH sensing and food Freshness monitoring. *Macromol. Mater. Eng.* **2026**, *311*, e00416. [CrossRef]
36. Gómez, S.; Lafiosca, P.; Giovannini, T. Modeling UV/ViS absorption spectra of food colorants in solution: Anthocyanins and curcumin as case studies. *Molecules* **2024**, *29*, 4378. [CrossRef] [PubMed]
37. Li, Q.; Zhang, F.; Wang, Z.; Feng, Y.; Han, Y. Advances in the preparation, stability, metabolism, and physiological roles of anthocyanins: A review. *Foods* **2023**, *12*, 3969. [CrossRef] [PubMed]
38. Janík, R.; Kohutiar, M.; Dubec, A.; Eckert, M.; Moricová, K.; Pajtášová, M.; Ondrušová, D.; Krbata, M. DMA analysis of plasma modified PVC films and the nature of initiated surface changes. *Materials* **2022**, *15*, 4658. [CrossRef] [PubMed]
39. Yuan, Z.; Chen, H.; Zhang, J. Facile method to prepare lotus-leaf-like super-hydrophobic poly(vinyl chloride) film. *Appl. Surf. Sci.* **2007**, *254*, 1593–1598. [CrossRef]
40. Li, X.; Chen, G.; Ma, Y.; Feng, L.; Zhao, H.; Jiang, L.; Wang, F. Preparation of a super-hydrophobic poly(vinyl chloride) surface via solvent–nonsolvent coating. *Polymer* **2005**, *47*, 506–509. [CrossRef]
41. Krongauz, V.V.; Getz, C.M.; Selin, V.V.; Boring, C.B. Kinetics of water vapor diffusion in plasticized poly(vinyl chloride). *J. Therm. Anal. Calorim.* **2026**, *151*, 17181–17199. [CrossRef]
42. Kim, M.; Cho, M.; Chung, C.; Kyung, K.-U. Stretchable, transparent and multifunctional PVC-gel heater: A novel approach to skin-mountable, wearable thermal devices. *npj Flex. Electron.* **2024**, *8*, 1–12. [CrossRef]
43. Minale, Y.F.; Gajdoš, I.; Szabo, T.; Kovács, A.P.; Major, A.Á.; Marossy, K.; Janowski, G. Thermal Behavior and Stability of PVC/TPU Blends Plasticized with a Bio-Based Plasticizer. *Thermo* **2026**, *6*, 26. [CrossRef]
44. Bakar, N.H.A.; Mazwir, M.H.; Ramli, R.M.; Khalil, M.; Ismail, W.N.W. Electrochemical detection of organophosphorus pesticides using screen-printed electrodes: A systematic literature review. *Anal. Methods* **2026**, *18*, 8550–8582. [CrossRef] [PubMed]
45. Li, Y.; Zhang, Z.; Zhu, H.; Sun, J.; Guo, M.; Zeng, X.; Li, Y.; Hashimoto, M. Plasticized PVC/CNT flexible electrodes for highly responsive, stable, and durable soft actuators and wearable sensors. *Sens. Actuators B Chem.* **2025**, *447*, 138894. [CrossRef]

46. Mishuk, M.N.; Hazra, M.; Kumar, A.; Dannberg, P.; Çakan, A.; Vogl, T. All-dry pick-up and transfer method for quantum emitter arrays in hexagonal boron nitride. *APL Photonics* **2025**, *10*, 0282288. [CrossRef]
47. Ratner, B.D.; Hoffman, A.S.; Schoen, F.J.; Lemons, J.E.; Wagner, W.R.; Sakiyama-Elbert, S.E.; Zhang, G.; Yaszemski, M.J. Introduction to Biomaterials Science. *Biomater. Sci.* **2020**, 3–19. [CrossRef]
48. Liu, Y.; Ge, L. Smart Biomaterials in Wound Healing: Advances, challenges, and future directions in intelligent dressing design. *Bioengineering* **2025**, *12*, 1178. [CrossRef] [PubMed]
49. Yang, X.; Zhang, M. Review of flexible microelectromechanical system sensors and devices. *Nanotechnol. Precis. Eng.* **2021**, *4*, 025001. [CrossRef]
50. Topol, E.J. High-performance medicine: The convergence of human and artificial intelligence. *Nat. Med.* **2018**, *25*, 44–56. [CrossRef] [PubMed]

Disclaimer/Publisher's Note: The statements, opinions and data contained in all publications are solely those of the individual author(s) and contributor(s) and not of MDPI and/or the editor(s). MDPI and/or the editor(s) disclaim responsibility for any injury to people or property resulting from any ideas, methods, instructions or products referred to in the content.